



Università degli studi di Napoli Federico II

Facoltà di scienze MM.FF.NN.

Dottorato di ricerca in fisica fondamentale e applicata

XIX ciclo

**A theoretical scenario for interpreting
present and future data
on young intermediate mass
pulsating stars**

Relatori:

Prof. Massimo Capaccioli

Dott.^{ssa} Marcella Marconi

Dott. Vincenzo Ripepi

Coordinatore:

Prof. Gennaro Miele

Candidato:

Alessandra Ruoppo

A Chiara

A mia mamma e mio padre

Contents

Introduction	v
1 An overview of Pulsating stars	1
1.1 Pulsating variable stars	1
1.2 The Physics of stellar pulsation	5
1.2.1 Stellar stability and Oscillations	5
1.2.2 Radial pulsation	6
1.3 Basic equations of pulsation	9
1.3.1 Equilibrium states and perturbation analysis	11
2 Physical properties of pre-main sequence stars	17
2.1 Pre Main sequence stars	17
2.2 Pre-Main-Sequence evolution	18
2.3 PMS δ Scuti stars	24
2.4 Present observational status	25
2.5 Present theoretical status	27
3 Theoretical tools to reproduce PMS δ Scuti pulsation	31
3.1 Evolutionary models	31
3.2 Pulsational approach	34
3.3 Asymptotic theory	35
3.4 Numerical Techniques	37
3.4.1 Difference Equations	38
3.5 The predicted pulsational frequencies:the case of VV Ser	39

4	A theoretical approach for the interpretation of pulsating PMS intermediate-mass stars	53
4.1	Large frequency separation	54
4.2	A methodology to reproduce the observed frequencies	56
4.2.1	The HR diagram	58
4.2.2	The large frequency separation and the echelle diagram	60
4.3	Application to observed PMS δ Scuti stars	63
4.3.1	The case of V351 Ori	63
4.3.2	The case of IP Per	67
4.4	Effects of rotation	69
5	Connection to the ESTA CoRoT activity	71
5.1	CoRoT ESTA	71
5.2	Comparisons among evolutionary codes	73
5.3	Pulsational frequency comparison	76
5.4	FRANEC PMS evolutionary models	81
6	Conclusion and future prospect	85
	References	89

Introduction

In the context of stellar evolution and pulsation my PhD thesis is devoted to the construction of a theoretical framework for the interpretation of present and future data on young intermediate mass pulsating stars. Pre-main sequence (PMS) stars with masses in the range from 1.5 to 4 M_{\odot} cross the pulsation instability strip of more evolved classical pulsators during their evolution toward the main sequence (MS) and, for this reason, it is expected that at least part of their activity could be due to pulsation.

The first evidence of δ Scuti pulsation in PMS stars was provided by Breger, (1972), who discovered two candidates in the young cluster NGC 2264. This evidence was confirmed more than 20 years later by Kurtz & Marang (1995) and Donati (1997) that observed this kind of pulsation in the Herbig Ae stars HR5999 and HD104237 respectively. The interest in this class of objects has grown up during the last decade and the current number of known or suspected candidates amounts to about 35 stars. However, only a few stars of the PMS δ Scuti class have been studied in detail, so that the overall properties of these pulsators are still poorly determined. In this context it is expected that the satellite CoRoT will be able to observe PMS δ Scuti stars with more accuracy as well as to discover new objects.

The investigation of the pulsation properties of Pre-main sequence intermediate mass stars is a promising tool to evaluate the intrinsic properties of these stars and to constrain current evolutionary models.

In this thesis I aim at developing a theoretical approach for the interpretation of observed frequencies, both from the already available ground-based observations and from the future more accurate and extensive CoRoT results in the context of CoRoT ESTA collaboration. To this purpose, I present a project devoted to the computations of fine and extensive grids of asteroseismic models of intermediate mass PMS stars. A linear adi-

adiabatic non-radial pulsation code is applied to the models of the grid in order to build a reference base to reproduce the observed pulsation frequencies. The obtained frequencies are used to derive an analytical relation between the large frequency separation and the stellar luminosity and effective temperature, and to develop a tool to compare theory and observations in the echelle diagram. The predictive capabilities of the proposed method are verified through the application to test stars. Then, the procedure is applied to true observations from multisite campaigns and it is verified that I am able to constrain the stellar parameters of the observed pulsators, in particular the mass, in spite of the small number of measured frequencies. The thesis is organized as follows:

- in Chapter 1 I describe the physical properties of pulsating stars and the adiabatic equations for computing pulsation periods, for both radial and non radial modes;
- in Chapter 2 the evolutionary and pulsational properties of pre-main-sequence δ Scuti stars are investigated, together with an outline of the present “theoretical” and “observational “ status;
- in Chapter 3 I present the evolutionary PMS models, introduce the non-radial pulsation code adapted by myself to PMS intermediate mass structures and report on the predicted pulsation frequencies. The computed large separation and its dependence on luminosity and effective temperature are discussed;
- in Chapter 4 I present a method to reproduce the observed frequencies and a theoretical test of the predictive capabilities of the method; I finally compare the theoretical results with the observations from multisite campaigns;
- in Chapter 5 I discuss the work done in the context of the CoRoT ESTA collaboration;
- Finally the Conclusions close the thesis.

An overview of Pulsating stars

In this chapter I describe the pulsating variable stars, their main characteristics. In particular I analyze the mechanisms responsible of pulsations, and finally the equations that consents of obtaining the pulsations periods both for radial and non radial motion.

1.1 Pulsating variable stars

A star is a self-gravitating gaseous sphere that radiates an enormous amount of energy to its outer space. Energy radiated from the surface is generated in the deep interior by thermonuclear reaction. A star is by no means a quiet object, but it is in a sense a kind of heat engine exhibiting various activities. Some stars blow out stellar winds from their surfaces, while some others are pulsating variables. A pulsating variable is a star that changes its brightness periodically by changing its volume.

It is interesting to study stellar pulsations for understanding why, and how, certain types of stars pulsate, but also because it is possible to use the pulsations to learn about the more general properties of the stars. In this work only intrinsic pulsators are analysed, that is stars whose luminosity varies periodically due to causes inside the stars themselves.

The first studies of pulsating stars initially were concentrated on stars with large amplitudes, such as the classical Cepheids and long period variables. The luminosity variations

of these stars could be understood in terms of radial pulsation with the star expanding and contracting, while preserving spherical symmetry.

The main emphasis in the early studies was on understanding the causes of the pulsations, particularly the concentration of pulsating stars in the *instability strip*. Important contributions to interpretation of stellar pulsation were made by Eddington (e.g. Eddington 1926), but the identification of the actual pulsation mechanism and of the reason for the instability strip, were achieved independently by Zhevakin (1953) and by Cox & Whitney (1958).

However, subsequently it has been realized that some stars pulsate in more complicated ways than the Cepheids. Often more than one mode of oscillation is excited simultaneously in a star; these modes may include both radial overtones, in addition to the fundamental, and *nonradial* modes, where the motion does not preserve spherical symmetry. The study of multiperiodic and non-radial pulsators is extremely important for attempts to use pulsations to learn about the properties of stars. In fact each observed period is in principle an independent measure of the structure of the star. So the amount of information about the star grows with the number of modes that can be detected.

The classical example is the Sun, where currently several thousand individual modes have been identified. *Helioseismology* is the science of learning about solar interior from the observed frequencies.

Most of observed solar oscillations have periods close to five minutes, considerably shorter than the fundamental radial period expected for the Sun. Both the solar five-minute oscillations and the fundamental radial oscillation are acoustic modes, or *p modes*, driven by pressure fluctuations. This kind of pulsations is expected in other similar stars, and they are the targets of *Asteroseismology*.

Pulsating stars are found in different evolutionary stages, so that they are located in different regions, covering a wide luminosity range in the *Hertzsprung-Russell* (HR) diagram, (see Fig. 1.1). The properties of the most important classes of pulsating stars are reported in Table 1.1.

Classical pulsating stars, including Cepheids, RR Lyrae, δ Scuti, are located in a quite narrow almost vertical region in the HR's diagram known as *instability strip* (see Fig. 1.1). The Cepheids are young (population I) stars with mass ranging from 3 to 12 M_{\odot} ,

Table 1.1: Physical properties of pulsating variables. The columns report, from left to right: The variable class, the pulsation period, the absolute visual magnitude, the visual magnitude amplitude, the spectral type, the population type and the evolutionary state.

Class	P (day)	M_V	A_V	S. Type	Pop.Type	E. phase
δ Cephei	1 \div 100	-7 \div 2	≤ 1.5	F6 -K2	I	blue loop
RR Lyrae	0.3 \div 1	0.0 \div 1.0	≤ 2	A2-F2	II	HB
W Vir	10 \div 50	-3 \div 1	≤ 1.5	F2-G6?	II	post-HB
BL Her	2 \div 10	-1 \div 0	≤ 1.5	F2-G6?	II	post-HB
AC	0.3 \div 2	-2 \div 0	≤ 1.5	A-F	? "young"	massive HB
SX Phoe	≤ 0.1	2 \div 3	≤ 0.5	A-F	Ii	MS
δ Scuti	≤ 0.5	2 \div 3	≤ 1.5	A-F	I	MS
β Ceph	≤ 0.3	-4.5 <i>div</i> -3.5	≤ 0.5	B1-B2	I	MS
Mira	$\div 50$	-2 \div 1	≥ 2.5	M_e, R_e, N_e, S_e	I,II	AGB
SR	100 \div 200	-3 \div 1	≤ 2.5	(K) _i M,R,N,S	I,II	AGB

that cross the instability strip, during the central helium burning phase. In particular they perform a blueward excursion in the HR diagram, known as *blue loop*. Thanks to their characteristic Period-Luminosity relations, discovered by Mrs Leavitt in 1912, Cepheids are the most important primary distance indicators within the Local Group. Moreover from the space they can be used to derive the distance of external galaxies and to calibrate various classes of secondary distance indicators. In this sense they are the basis of an absolute extragalactic distance scale.

RR Lyrae, instead, are low mass ($\lesssim 0.8 M_\odot$), population II pulsating stars during the so called *horizontal-branch* (HB) phase, that is the phase of central helium burning for low mass stars. They are observed in globular clusters, in the Galactic halo, and are concentrated toward the Galactic center.

The absolute magnitude of RR Lyrae and its dependence on metal abundance, make them useful standar candles for population II systems. On this basis they can be used to calibrate some secondary distance indicators such as the globular cluster luminosity function. At the same time they are excellent tracers of the chemical and dynamical properties of old

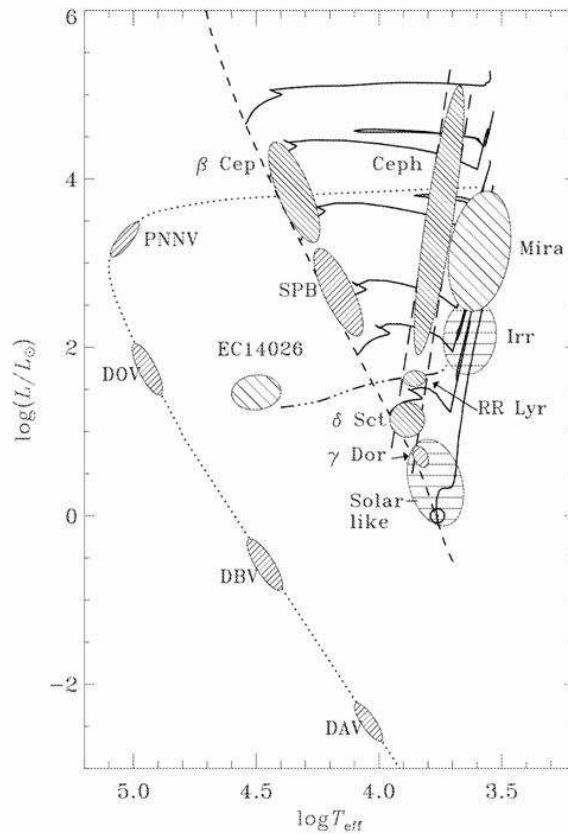


Figure 1.1: HR diagram with the position of most common pulsating variable stars.

stellar populations. Beyond RR Lyrae other important classes of radial pulsators are actually observed in globular clusters and similar metal-poor stellar fields. According to the current nomenclature we find Population II Cepheids (PII Cs) and anomalous Cepheids (ACs). These two classes are interpreted as helium burning structures both brighter either less massive (PII Cs) or more massive (ACs) than RR Lyrae with similar metal content. Another important class of pulsating star is the δ Scuti one. δ Scuti stars are pulsators located in the classical instability strip close to the main sequence* or moving from the main sequence to the red giant branch.† In general their period varies from 0.02d to 0.025d. Some δ Scuti stars are pure radial pulsators, while the majority pulsate with a large number of nonradial p -modes simultaneously for this reason δ Scuti stars represent a transition class between the cepheid-like large-amplitude radial pulsators and the non-radial pulsators located in the hot part of the HR diagram.

*A star on the main sequence is one that is generating light and heat by the conversion of hydrogen (1^H) to helium 4^He by nuclear fusion in its core.

†Red Giant Branch stars are burning hydrogen in a shell surrounding a dormant helium core.

A recently discovered class of δ Scuti pulsating stars is represented by the Pre-Main sequence (PMS) stars. They are intermediate mass ($1.5M_{\odot} < M < 4M_{\odot}$) stars that cross the pulsation instability strip of more evolved classical pulsators during their evolution toward the Main Sequence (MS). The pulsation of this class of stars is the main argument of this work, and their properties will be described in detail in the Chapter 2.

Other pulsating classes of stars that shown both radial and non-radial oscillations are β Cepheid and γ Doradus stars. They are main sequence stars (or close), with oscillate probably with gravity modes, that is non radial modes in which the restoring force is the gravity. The rapidly oscillating Ap stars are also located in the instability strip, they oscillate in high-order acoustic modes, rather like the Sun, but the oscillations are closely tied to the large-scale magnetic field found in these stars.

Red giants show oscillations of very long periods, corresponding to the large dynamic timescale resulting from their huge radii. In this evolutionary phase Mira variables have very large amplitudes in the visible band, up to eight magnitudes, although the amplitude in the luminosity oscillations are more modest. They are typically single periodic. Other red giant pulsators are irregular variables with lower amplitudes and amplitudes and possibly period variations.

In the final stages of stellar evolution we find the subdwarf B variable stars, and the pulsating white dwarfs.

1.2 The Physics of stellar pulsation

1.2.1 Stellar stability and Oscillations

Three types of stability are fundamental for the equilibrium configuration of a star:

- dynamical stability;
- thermal stability;
- vibrational stability.

The dynamical stability is verified when for an arbitrary small contraction of a star as a whole, the increment of pressure gradient exceeds that of the gravitational force, and the

equilibrium structure is restored. In this state of dynamical stability the stars should spend almost all their lives.

Thermal stability is verified when an excess input of thermal energy causes a perfect gas star to expand as the virial theorem implies, and the temperature is normally decreased by hydrostatic adjustment. This is the state of thermal stability.

A dynamically stable system undergoes oscillation if perturbation is applied to it. An oscillation of a system may or may not grow in time. If it grows, it is said to be vibrationally (or pulsationally) unstable. In order for an oscillatory stable system to maintain a regular periodic oscillation, external force must be applied periodically. This is a forced oscillation, on the other hand, free oscillations will continue for at least some time once a perturbation has been applied initially. In the following the physical properties of radial and nonradial free oscillations of stars are described .

1.2.2 Radial pulsation

The radial oscillations of a pulsating star are the result of sound waves resonating in the star's interior. A rough estimate of the pulsation period, Π , may easily be obtained by considering how long it would take a sound wave to cross the diameter of a model star and gives:

$$\Pi \approx \sqrt{\frac{3\pi}{2\gamma G\rho}} \quad (1.1)$$

where ρ is the star density, and γ and G , the ratio of specif heats ($\gamma = \frac{C_p}{C_v}$) and the gravitational constant respectively. Qualitatively, this show that the pulsation period of a star is inversely proportional to the square root of its mean density.

This *period-mean density relation* explains why the pulsation periods decrease as you move down the instability strip from the very tenuous supergiants to the very dense white dwarfs.

The sound waves involved in the radial modes of stellar pulsation are essentially *standing waves*, and a star can have several modes of oscillation. In the *fundamental mode* the gas moves in the same direction at every point in the star, while in the *first overtone* mode, there is a single node with the gases moving in opposite directions on either side of the node.

To explain the mechanism that powers these standing waves, Eddington proposed that pulsating stars are like thermodynamic heat engine. The gases comprising the layers of the stars do work as they expand and contract throughout the pulsation cycle. If the work on a cycle is positive, the layer does net work on its surroundings and contributes to driving the oscillations; otherwise the layer tends to damping the oscillations.

As for any heat engine, the net work done by each layer of the star during one cycle is the difference between the heat flowing into the gas and the heat leaving the gas. For driving, the heat must enter the layer during the high-temperature part of the cycle and leave it during the low-temperature part.

To explain in what region of the star the driving take place, Eddington suggested a *valve mechanism*. If a layer of the star became more opaque upon compression, it could “dam up” the energy flowing toward the surface and push the surface layers upward. Then, as this expanding layer became more transparent, the trapped heat could escape and the layer would fall back down to begin the cycle anew. In Eddington’s own words, “To apply this method we must take the star more heat-tight when compressed than when expanded; in other words, *the opacity must increase with compression*”.

In most regions of the star, however, the opacity decreases with compression. In fact the opacity k depends on the density and temperature of the stellar material as $k \propto \frac{\rho}{T^{3.5}}$ (Kramers law). As the layers of a star are compressed, their density and temperature both increase. But as the opacity is more sensitive to the temperature than to the density, the opacity of the gases usually decreases upon compression. It takes special circumstances to overcome the damping effect of most stellar layers, which explains why stellar pulsation is observed for only one of every 10^5 stars.

The special conditions responsible for exciting and maintaining the stellar oscillations were first identified by the Russian astronomer S. A. Zhevakin and verified in detailed calculations by Kippenhahn, Baker and Cox. They found that the regions of a star where Eddington’s valve mechanism can successfully operate are its *partial ionization zones*. In these layers of the star where the gases are partially ionized, a significant part of the work done on the gases as they are compressed produce further ionization rather than raising the temperature of the gas. With a smaller temperature rise, the increase in density with compression produces a corresponding increase in Kramers opacity. Similar

during expansion, the temperature does not decrease as much as expected since the ions now recombine with electrons and release energy. Again, the density term in Kramers law dominates, and the opacity decreases with decreasing density during expansion. This layer of the star can thus absorb heat during compression, be pushed outward to release the heating during expansion, and fall back down again to begin another cycle. This mechanism is known as *k-mechanism*. In a partial ionization zone, the k-mechanism is reinforced by the tendency of heat to flow into the zone during compression simply because its temperature is lower than in the adjacent stellar layers. This effect is called *γ -mechanism*, after the smaller ratio of specific heats caused by the increased values of C_p and C_v . Partial ionization zones modulate the flow of energy through the layers of the star and are the direct cause of stellar pulsation.

In most stars there are two main ionization zones. The *hydrogen partial ionization zone* where both the ionization of neutral hydrogen ($H \rightarrow HI$) and the first ionization of helium ($HeI \rightarrow HeII$) occurs in layers with a characteristic temperature of $1.5 \cdot 10^4 K$. The second, deeper zone is called the *He II partial ionization zone*, and involves the second ionization of helium ($HeII \rightarrow HeIII$), which occurs at a characteristic temperature of $4 \cdot 10^4 K$. The location of these ionization zones within the star determines its pulsational properties. In fact if the star is too hot ($\gtrsim 8000 K$), the pulsation is not active, because the ionization zones will be located very near to the surface. In this region the density is quite low and there is not enough mass available to drive the oscillations. This explains the blue (hot) edge of the instability strip on the H-R diagram. Otherwise if a star's surface temperature is too low ($\lesssim 5500 K$), the onset of efficient convection in its outer layers may dampen the oscillations. Because the transport of energy by convection is more efficient when the star is compressed, the convective stellar material may lose heat at minimum radius. This could overcome the damming up of heat by the ionization zones, and so inhibit the pulsation of the star. The red (cool) edge of the instability strip is believed to be the result of the damping effect of convection.

The mechanism responsible for the pulsation of stars outside the classical instability strip is not as well understood.

1.3 Basic equations of pulsation

In this section I present the basic equations governing radial and non-radial oscillations. I assume that the gas can be treated as continuum, so that the equations of the stellar interiors are the same of a general fluid.

I neglect viscosity and assume that gravity is the only body force, so that, for example, magnetic fields are neglected. Then the equation of motion can be written as:

$$\rho \frac{D\vec{v}}{Dt} = -\nabla p + \rho \nabla \Phi \quad (1.2)$$

where \vec{v} is the velocity, p is the pressure, ρ is the density, and Φ is the gravitational potential. As usual D/Dt denotes the material time derivative ($Df/Dt = \partial f/\partial t + \vec{v} \cdot \nabla f$).

The density satisfies the equation of continuity,

$$\frac{D\rho}{Dt} = -\rho \operatorname{div} \vec{v} \quad (1.3)$$

and Φ is determined by Poisson's equation,

$$\nabla^2 \Phi = -4\pi G \rho \quad (1.4)$$

where G is the gravitational constant.

To complete the equation system a relation between p and ρ has been computed. This is determined by the energy equation:

$$\frac{dq}{dt} = \frac{dE}{dt} + p \frac{dV}{dt} \quad (1.5)$$

here $\frac{dq}{dt}$ is the rate of heat loss or gain, and E the internal energy per unit mass. The equation 1.5, expresses the fact that the heat gain goes partly to change the internal energy, partly into work expanding or compressing the gas.

By using the equation of continuity and thermodynamic identities, the energy equation can be expressed in terms of other more convenient variables.

$$\frac{dq}{dt} = \frac{1}{\rho(\Gamma_3 - 1)} \left(\frac{dp}{dt} - \frac{\Gamma_1 p}{\rho} \frac{d\rho}{dt} \right) = c_v \left[\frac{dT}{dt} - (\Gamma_3 - 1) \frac{T}{\rho} \frac{d\rho}{dt} \right] \quad (1.6)$$

Here c_v is the specific heat per unit mass at constant volume, and $\Gamma_1 = \left(\frac{\partial \ln p}{\partial \rho} \right)_{ad}$, and $\Gamma_3 - 1 = \left(\frac{\partial \ln T}{\partial \rho} \right)_{ad}$ are two adiabatic exponents.

It is evident that the relation between p , ρ and T , as well as Γ_i 's, depend on the thermodynamic state and composition of the gas.

Now it has been considered the heat gain in more detail. Specifically it can be written as:

$$\rho \frac{dq}{dt} = \rho \epsilon - \text{div} \vec{F} \quad (1.7)$$

where ϵ is the rate of energy generation per unit mass, and \vec{F} is the flux of energy. In general, radiation is the only significant contributor to the energy flux.

In convective zones turbulent gas motion provides a very efficient transport of energy. Ideally the entire hydrodynamical system, including convection, must be described as a whole. In this case only the radiative flux would be included in equation 1.7. However, under most circumstances the resulting equations are too complex to be handled analytically or numerically. Thus it is customary to separate out the convective motion, by performing averages of the equations over length scales that are large compared with the convective motion, but small compared with other scales of interest. In this case the convective flux appears as an additional contribution in equation 1.7. The convective flux must then be determined, from the other quantities characterizing the system, by considering the equation for the turbulent motion. A familiar example of this is the mixing-length theory.

The general calculation of the radiative flux is also non-trivial. In stellar interiors the diffusion approximation is adequate, and the radiative flux is given by:

$$\vec{F} = -\frac{4acT^3}{3k\rho} \nabla T \quad (1.8)$$

where k is the opacity, c is the speed of light and a is the radiation density constant; this provides a relation between the state of the gas and the radiative flux.

For purpose of calculating stellar oscillation frequencies, the complication of the energy equation can be avoided to a high degree of precision, by neglecting the heating term in the energy equation. When the heating can be neglected, the motion occurs *adiabatically*.

Then equation 1.7 becomes:

$$\frac{dp}{dt} = \frac{\Gamma_1 p}{\rho} \frac{d\rho}{dt} \quad (1.9)$$

The adiabatic approximation is evidently highly restrictive. In particular, the motion is conservative, and hence the total energy is constant. Thus, when considering a single mode of oscillation in the adiabatic approximation, the amplitude of the mode is constant, and

therefore it is not possible to treat its excitation or damping. The nonadiabatic effects also modify the dynamical properties of the motion and hence affect the oscillation frequencies, by small but not negligible amounts.

The equation 1.9, together with the continuity equation 1.3, the equation of motion 1.2 and Poisson's equation 1.4, form the complete set of equations for adiabatic motion.

1.3.1 Equilibrium states and perturbation analysis

A general hydrodynamical description of a star, using the equations described, in the previous subsection, is far too complex to handle, even numerically on the largest existing computers.

Luckily, in the case of stellar oscillations, considerable simplifications are possible. The observed solar oscillations have very small amplitudes compared with the characteristic scales of the Sun, and so it can be treated as a small perturbation around a static equilibrium state. Even in "classical" pulsating stars, where the surface amplitudes are relatively large, most of the energy in the motion is in regions where the amplitudes are smaller; thus many of the properties of these oscillations, in particular their periods, can be understood in terms of small-perturbation theory.

The equilibrium structure is assumed to be static, so that all time derivatives can be neglected, and it is assumed that there are no velocities.

Then the equation of motion 1.2 reduces to the equation of hydrostatic support,

$$\nabla p_0 = \rho_0 \vec{g}_0 = -\rho_0 \nabla \Phi_0 \quad (1.10)$$

where the subscript "0" denotes equilibrium quantities. Then the continuity equation 1.3, is trivially satisfied. Poisson's equation 1.4 is unchanged,

$$\nabla^2 \Phi_0 = 4\pi G \rho_0 \quad (1.11)$$

Finally the energy equation 1.7 is:

$$0 = \frac{dq}{dt} = \epsilon_0 - \frac{1}{\rho_0} \text{div} \vec{F}_0 \quad (1.12)$$

The most important example of equilibrium is clearly a spherically symmetric state, where the structure depends only on the distance r to the centre. Here $\vec{g}_0 = -g_0 \hat{a}_r$, where \hat{a}_r is

a unit vector directed radially outward, and the equation 1.10 becomes:

$$\frac{dp_0}{dr} = -g_0\rho_0 \quad (1.13)$$

Integrating once Poisson's equation:

$$g_0 = \frac{Gm_0(r)}{r^2} \quad (1.14)$$

where $m_0(r)$ is the mass interior to r . The flux is directed radially outward, $\vec{F} = F_{r,0}\hat{a}_r$, so that the energy equation gives:

$$\rho_0\epsilon_0 = \frac{1}{4\pi r^2} \frac{dL_0}{dr} \quad (1.15)$$

where $L_0 = 4\pi r^2 F_{r,0}$ is the total flow of energy through the sphere with radius r .

Finally the diffusion expression for the flux may be written:

$$\frac{dT_0}{dr} = -\frac{3K_0\rho_0}{16\pi r^2 acT_0^3} L_0 \quad (1.16)$$

Equations 1.13 - 1.16 are clearly the familiar equations for stellar structure.

Now it is considered small perturbations around the equilibrium state. Thus, e.g., the pressure is written as:

$$p(\vec{r}, t) = p_0 + p'(\vec{r}, t) \quad (1.17)$$

where p' is a small perturbation; this is the so-called *Eulerian* perturbation, that is the perturbation at a given point. The equations are then linearized in the perturbations, by expanding them in the perturbations, retaining only terms that do not contain products of the perturbations. The linearized equations are written as follows:

For the momentum equation:

$$\rho_0 \frac{\partial^2 \delta \vec{r}}{\partial t^2} = -\nabla p' + \rho_0 \vec{g}' + \rho' g_0 \quad (1.18)$$

For the continuity equation:

$$\frac{\partial \rho'}{\partial t} + \text{div}(\rho_0 \vec{v}) \quad (1.19)$$

For Poisson's equation:

$$\nabla^2 \Phi' = 4\pi G \rho' \quad (1.20)$$

Finally for adiabatic motion, the linearized energy equation is given by:

$$p' + \vec{\delta r} \cdot \nabla p_0 = \frac{\Gamma_{1,0} p_0}{\rho_0} (\rho' + \vec{\delta r} \cdot \nabla \rho_0) \quad (1.21)$$

Because of the spherical symmetry and the time independence of the equilibrium mode, it is possible to separate the perturbation quantities in spherical polar coordinates (r, θ, ϕ) and time. The equation can be combined in such a way that all derivatives with respect to θ and ϕ appear in the form of the tangential Laplace operator:

$$\nabla_t^2 = \frac{1}{r^2 \sin \theta} \frac{\partial}{\partial \theta} \left(\sin \theta \frac{\partial}{\partial \theta} \right) + \frac{1}{r^2 \sin^2 \theta} \frac{\partial^2}{\partial \phi^2} \quad (1.22)$$

In this case, the separation of variables into radial and angular parts is possible for all the variables, with the angular dependence of $Y(\theta, \phi)$ satisfying:

$$[r^2 \nabla_t^2 + \Lambda] Y(\theta, \phi) = 0 \quad (1.23)$$

where Λ is a constant.

It is possible to show that $Y(\theta, \phi)$ may be chosen as a spherical harmonic Y_l^m defined by:

$$Y_l^m(\theta, \phi) = (-1)^m c_{lm} P_l^m(\cos \theta) e^{im\phi} \quad (1.24)$$

where $m = -l, -l+1, \dots, l-1, l$, $\Lambda = l(l+1)$ with l integer, P_l^m is a Legendre function, and c_{lm} is determined by:

$$c_{lm}^2 = \frac{2l+1}{4\pi} \frac{(l-m)!}{(l+m)!} \quad (1.25)$$

such that the integral of $|Y_l^m|^2$ over the unit sphere is equal to one. On this basis, the displacement vector, and the pressure perturbation can be written as:

$$\delta \vec{r}(r, \theta, \phi, t) = \sqrt{4\pi} \text{Re} \left[\xi_r(r) Y_l^m \hat{a}_r + \xi_t(r) \left(\frac{\partial Y_l^m}{\partial \theta} \hat{a}_\theta + \frac{1}{\sin \theta} \frac{\partial Y_l^m}{\partial \phi} \hat{a}_\phi \right) \right] e^{-i\omega t} \quad (1.26)$$

$$p'(r, \theta, \phi, t) = \sqrt{4\pi} \text{Re} [p(r) Y_l^m(\theta, \phi) e^{-i\omega t}] \quad (1.27)$$

where \hat{a}_θ and \hat{a}_ϕ are unit vectors in the θ and ϕ direction.

By substituting the spherical harmonic representations into Eqs. 1.18 - 1.21, the following relations between the amplitude functions are obtained:

$$-\omega^2 \rho_0 \xi_r = -\frac{dp'}{dr} - \rho' g_0 - \rho_0 \frac{d\Phi'}{dr} \quad (1.28)$$

$$\omega^2[\rho' + \frac{1}{r^2} \frac{d}{dr}(r^2 \rho_0 \xi_r)] = \frac{l(l+1)}{r^2} (p' + \rho_0 \Phi') \quad (1.29)$$

$$\rho' = \frac{-1}{r^2} \frac{d}{dr}(r^2 \rho_0) + \frac{l(l+1)}{r} \rho_0 \xi_t \quad (1.30)$$

$$\frac{1}{r^2} \frac{d}{dr} (r^2 \frac{d\Phi'}{dr} - \frac{l(l+1)}{r^2} \Phi') = 4\pi G \rho \quad (1.31)$$

$$\rho' = \frac{\rho_0}{\Gamma_1 p_0} p' + \rho_0 \xi_r (\frac{1}{\Gamma_1 p} \frac{dp}{dr} - \frac{1}{\rho_0} \frac{d\rho}{dr}) \quad (1.32)$$

The last equation, that is the adiabatic energy equation, may be used to eliminate ρ' from equations 1.28 - 1.31, so that it is obtained a fourth-order system of ordinary differential equations for the four dependent variables ξ_r , p' , Φ' and $\frac{d\Phi'}{dr}$. On this basis it is shown the complete set of differential equations:

$$\frac{dp'}{r} = \rho_0 (\omega^2 - N^2) \xi_r + \frac{1}{\Gamma_1 p} \frac{dp}{dr} p' - \rho_0 \frac{d\Phi'}{dr} \quad (1.33)$$

where, N is the buoyancy frequency, given by:

$$N^2 = g (\frac{1}{\Gamma_1 p} \frac{dp}{dr} - \frac{1}{\rho} \frac{d\rho}{dr}) \quad (1.34)$$

$$\frac{d\xi_r}{dr} = -(\frac{2}{r} + \frac{1}{\Gamma_1 p} \frac{dp}{dr}) \xi_r + \frac{1}{\rho_0 c^2} (\frac{S_l^2}{\omega^2} - 1) p' + \frac{l(l+1)}{\omega^2 r^2} \Phi' \quad (1.35)$$

where $c^2 = \frac{\Gamma_1 p}{\rho}$ is the square of adiabatic sound speed and S_l the characteristic acoustic frequency defined by:

$$S_l^2 = \frac{l(l+1)c^2}{r^2} \quad (1.36)$$

Finally the Poisson's equation becomes:

$$\frac{1}{r^2} \frac{d}{dr} (r^2 \frac{d\Phi'}{dr}) = 4\pi G (\frac{p'}{c^2} + \frac{\rho_0 \xi_r}{g} N^2) + \frac{l(l+1)}{r^2} \Phi' \quad (1.37)$$

This set of differential equation is the start point for the description of linear adiabatic non radial oscillations.

For *radial* oscillations, with $l = 0$, the set of equation is reduced to a second-order system of differential equations, that is:

$$\frac{d\Phi'}{dr} = 4\pi G \rho \xi_r \quad (1.38)$$

$$\frac{1}{r^3} \frac{d}{dr} (r^4 \Gamma_1 p) \frac{d\xi_r}{dr} + \frac{d}{dr} [(3\Gamma_1 - 4)p] r \xi_r + \rho \omega^2 \xi_r \quad (1.39)$$

A nonzero solution to Eqs. 1.33 - 1.37, with the boundary conditions is possible for selected values of ω^2 , which is therefore an *eigenvalue* of the problem. For each value of l , one obtains a discrete spectrum of eigenfrequencies ω_{nl} , labeled by the radial order n . The eigenfrequencies depend on l but are degenerate by $(2l + 1)$ -folds in m . The normal modes belonging to the harmonic index l are further distinguished by the number of nodes, n , in the radial component of displacement from the center to surface of a star. The n -values are 0 for the fundamental mode, 1 for the first overtone mode, 2 for the second overtone mode, etc. The normal modes are classified by the radial number n and the angular number l . If the star rotates or it is considered the magnetic field, then the azimuthal number m has to be added, and the frequencies are splitted in a sort of “Zeeman splitting” of the atomic energetic level.

The richness of nonradial oscillations compared with the radial pulsation is partially due to the degree of freedom in the horizontal wave number represented by the harmonic degree l . There is also the physical reason that not only the pressure but also gravity can act as the restoring force causing nonradial oscillations. Since the change in the gravitational force is inward in the compressed phase, or outward in the expanded phase, gravity cannot be the restoring force for radial pulsation. On the other hand, gravity can act through buoyancy as the restoring force for nonradial oscillations. Thus, while the radial oscillations has only the spectrum of the pressure mode (p -mode, classified by $n > 0$) or acoustic mode, the nonradial oscillations shows the spectrum of the gravity mode (g -mode, classified by $n < 0$) as well. The behaviors of the p - and the g -mode oscillations are determined by the internal structure of stars.

Physical properties of pre-main sequence stars

In this chapter I analyze the PMS stars, with particular attention to the intermediate mass ones. In particular I describe the evolutionary phase of PMS stars and the pulsational behavior. At the end I summarize the present status of δ Scuti PMS stars both from an observational point of view than from a theoretical one.

2.1 Pre Main sequence stars

The study of the first stages in the formation of stars is one of the currently most active research fields in stellar astronomy. Pre-main sequence (PMS) stars are usually found within star formation regions and they are characterized by a high degree of activity, with the presence of winds, jets, outflows etc. They are interacting with the circumstellar environment in which they are embedded. Mostly they have strong infrared and/or UV excesses and show photometric and spectroscopic variability on time scales from minutes to years. On time scales of weeks to hours the phenomenon is generated by variable extinction due to circumstellar dust, clumped accretion and chromospheric activity. On time scales of half an hour to some hours the variation may be due to pulsation if the star lies

in or near the instability strip. Stars over essentially the whole mass spectrum can become pulsationally unstable during various stages of their evolution. The fact that young stars during their evolution to the main sequence move across the instability region raises the possibility that at least part of the observed stellar activity could also be due to stellar pulsations. The discovery of pulsation in PMS stars is extremely important, since it provides a unique means for constraining the internal structure of young stars and for testing evolutionary models. Although it is difficult to put constraints on the characteristics of young stars and to define whether they are in their PMS phase of evolution or not, two different types of (possible) PMS objects can be identified, namely the T Tauri and Herbig Ae/Be stars. T Tauri stars are newly formed low-mass stars that have recently become visible in the optical range. Joy 1942 first discovered this group of stars in the Taurus-Auriga dark cloud and named them after their brightest member 'T Tauri'. They are PMS stars of late spectral type (G, K and M). They show apparently normal photospheres overlain by continuum and line-emission characteristics of a hotter (about 7000 K to 10000 K) envelope. T Tauri stars display irregular and large light variations and are associated with the dark or bright nebulae from which they were born. As they are of late spectral types they do not provide the necessary scenario for the κ mechanism for driving pulsation. Herbig Ae/Be stars, are intermediate mass pre-main-sequence stars. In 1960 Herbig suggested that "Be and Ae stars associated with nebulosity" are PMS stars of intermediate mass ($2 - 10M_{\odot}$) in their radiative phase of contraction toward the main sequence. Herbig Ae/Be (HAEBE) stars are characterized by the following properties: 1) hot emission line; 2) spectral type B, A or F; 3) a near- or far-IR excess.

In the following section we describe the evolution of both low and intermediate mass stars. The remaining part of the chapter is devoted to the properties of pulsation intermediate mass PMS stars.

2.2 Pre-Main-Sequence evolution

The pre-main-sequence (PMS) contraction of stars of all masses is a well established phase of stellar evolution. The first studies of this phase of stellar evolution are due to Hayashi, Henyey, Iben, Cameron and their collaborators in the early 1960s.

The pre-main sequence phase of stellar evolution represents the last period of a star's youth, before the object begins the hydrogen fusion. As the star begins pre-main-sequence contraction, it is no longer buried within an opaque dust cloud and radiation can emanate freely from the surface layers. The star becomes a “mature” object and it is relatively easy to observe by traditional means.

The early phases of stellar evolution are strongly influenced by the conditions inherited by the stars during the process of star formation. In particular, the PMS “history” begins with the initial conditions set by protostellar evolution which also determines the time $t_0 = t_{proto}$ for PMS models. Therefore, before describing the PMS evolution, here it is summarized the most important properties of protostars. The formation of a protostars from the quiescent conditions of dense cores occurs through the gradual accumulation of the interstellar gas onto an accreting core. This process requires a large decrease in gravitational potential energy. A large fraction of this energy is radiated away in radial or disk accretion shocks that form as a result of the violent change in the velocity of the freely-falling gas. If no net energy is absorbed by the circumstellar material, the resulting luminosity is given to a good approximation by :

$$L_{acc} = \frac{GM_*\dot{M}_{acc}}{R_*} \quad (2.1)$$

where M_* and R_* are the instantaneous mass and radius of the protostellar core, and $\dot{M}_{acc} = \frac{dM_*}{dt}$ the mass accretion rate. Thus, estimates of the luminosity emitted during this phase rely on the knowledge of two fundamental quantities, *the mass accretion rate*, and the *mass-radius relation*. The former is determined by the dynamics of the gravitational collapse, while the relation between the mass and the radius are established by processes occurring in the protostellar interior. The radiation produced at the shock is absorbed, radiated and thermalized in the optically thick dusty infalling envelope. Most of the observable radiation is emitted at mid- and far-infrared wavelengths.

The properties of accreting protostars have been determined by several authors (e.g. Stahler 1988; Palla & Stahler 1991, 1992; Beech & Mitalas 1994; Bernasconi & Maeder 1996; Siess et al. 1997; Norberg & Maeder 2000). Some of the main results of these initial models are listed below:

- The typical radii of protostars ($\sim 5R_\odot$ for $1M_\odot$) are an order of magnitude smaller

than those assumed in the first study of PMS evolution such as the once performed by Hayashi and his collaborators;

- For low- and intermediate-mass protostars is verified a *mass-radius* relation. The key physical process that maintains such relation is the nuclear burning of the interstellar deuterium contained in minute abundances ($\sim 10^{-5}$ relative to hydrogen) in the accreted gas mixture;
- This mass-radius relation can be used to build a *birthline* for stars in the HR diagram: the birthline is the region where young stars first appear as optically visible stars;
- A prediction of this models is that the birthline intersects the Zero Age Main Sequence (ZAMS) at a mass of $\sim 10M_{\odot}$. Thus stars with mass greater than $10M_{\odot}$, have no a pre-main-sequence phase, because they become optically visible when they have initiated hydrogen yet, that is they are born on the ZAMS.

As the protostar grows in both size and mass, deuterium eventually ignites and drives convection for low-mass object ($M_* \lesssim M_{\odot}$). Convection ceases in the intermediate-mass protostars, while deuterium continues to burn in a interior shell. If accretion continues, the protostar contracts, and heats up until ordinary hydrogen ignites.

Disks arise during protostellar evolution from infalling material with too much angular momentum to impact the star itself. These geometrically thin structures expand rapidly with the time. Qualitatively, the global effect of accretion through a disk is to yield matter landing into the star with a lower specific entropy than that which hits the surface directly, because of the heat loss through radiation from the disk faces.

Once the main phase of accretion is completed, the stellar core becomes an optically visible star along the birthline. The physical process by which infall stops is still not known, although stellar winds and bipolar outflows must play a fundamental role. The circumstellar matter surrounding these young stars, partly distributed in a disk and the rest in an extended envelope, still emits at infrared wavelengths, whose spectral energy distribution is different from a normal stellar one because of the excess emission extending from the near- to the far-infrared.

A pre-main-sequence star loses internal energy from its surface layers, by emitting radiation. Since the object is gravitationally bound, its total energy, E_{tot} , is negative and

increases in absolute value with time. The thermal contribution K is positive, in fact, thanks to the virial theorem ($2K + U = 0$ where U is the internal energy), it is equal to $-E_{tot}$. Thus, the thermal energy and the temperature actually increase. A pre-main sequence star, as the other stars, is an object with negative heat capacity, one whose the temperature increases as result of heat loss. This behaviour occurs because of the increased gravitational binding.

Pre-main sequence stars can be treated at each instant as objects in hydrostatic and thermal equilibrium. In fact the energy loss from radiation causes the contraction of the star with the characteristic time scale of Kelvin Helmholtz T_{KH}^* , but the stellar interior readjust to maintain force balance. This readjustment is achieved through pressure perturbations and take place over the sound travel time, $t_s = \frac{R_\odot}{a_s}$, where a_s is an appropriately averaged sound speed. The justification for the evolution to be quasi static is that $t_{KH} \gg t_s$ throughout the pre-main-sequence phase.

On this basis the calculation of pre-main-sequence evolution utilizes the four, first order differential equation of stellar structure(see cap1, 1.13 - 1.16) together with the boundary conditions: $M = 0: r(0) = 0; L_{int}(0) = 0; M = M_*: L_{int}(M_*) = 4\pi R_*^2 \sigma_B T_{eff}^4; P_{M_*} = \frac{2GM_*}{3R_*^2 k_{phot}}$, the last condition derives from the assumptions that $P(M_*)$ must equal the appropriate photospheric value when $M_r = M_*$.

The full four stellar structure equations must be solved as a two-point boundary value problem, in which the values of pressure and entropy are guessed at the center, while the stellar radius and luminosity are guessed at the surface. One can integrate the equations from both directions to an interior fitting point, where the four guesses must be changed until all variables match.

The evolutionary tracks for pre-main-sequence stars, as calculated by Palla & Stahler (1993), are plotted in the HR diagram from masses ranging from 1 to 6 M_\odot , see fig. 2.1 For T Tauri stars (low mass stars $1 < \frac{M}{M_\odot} < 2$), it could be noticed that the star's emitted luminosity is initially high enough to drive interior convection. Mixing associated with turbulent convection enforces a spatially constant specific entropy, and the star

*If a star is not in equilibrium, that is there are no force to opposing the gravitational collapse, it would slowly contract, radiating away all of its gravitational potential energy. If it does so at its luminosity L , the time it takes to radiate away its energy is given by the total energy divided by the rate the energy is lost (which is the luminosity). This time, is given by $t_{KH} = GM^2/RL$

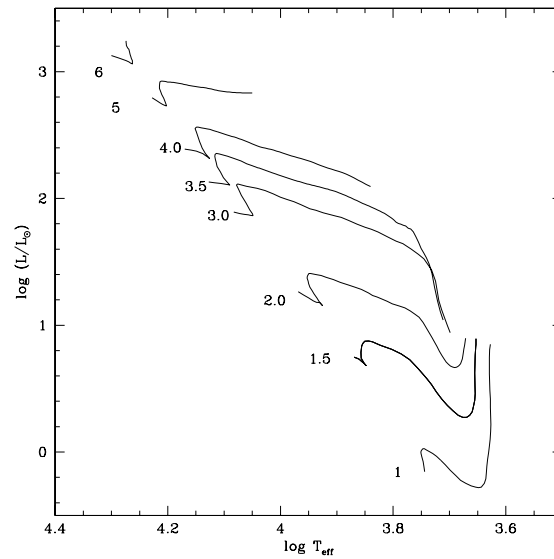


Figure 2.1: Evolutionary tracks for PMS stars.

contracts in a simple, homologous fashion. Since the effective temperature remain nearly fixed, the objects descends vertically in the HR diagram. Eventually, the interior opacity diminishes to the point where radiation can provide energy transport. The effective temperature then increases, and the evolutionary tracks become more horizontal.

The rising central temperature in a pre-main sequence star ignites a sequence of nuclear reactions. First, the object exhaust whatever deuterium remains from the protostar phase. This reaction can stall contraction for up to 10^6 years in the lowest-mass stars. The subsequent fusion of lithium is energetically trivial. Ordinary hydrogen eventually burns in all stars more massive than $0.075M_{\odot}$. Here, the released energy completely halts stellar contraction.

Objects of even smaller mass have a central temperature that pecks too low for hydrogen ignition and then declines further as the radius settles to a finite value. These stars are known as brown dwarfs, in which the electron degeneracy pressure counteracts self-gravity.

The evolution of Herbig Ae/Be is influenced more than the one of T Tauri by the prior accretion hystory and strongly depends on the stellar mass range. Three different regimes can be identified:

- Stars in the range from 1 to $2.5M_{\odot}$ are *fully convective stars*, due to surface cooling,

as soon as they appear as optically visible objects. The evolution is undisturbed by the fusion of residual deuterium: its concentration is so low, that it is quickly consumed. They contract along the Hayashi track[†], but their path is much reduced with respect to the T Tauri;

- Stars in the range from 2.5 to $4M_{\odot}$ are *partially convective stars*. They undergo thermal relaxation and nonhomologous contraction. When they are first optically visible, they are *underluminous*, that is the star begins with a modest surface luminosity and then moves up to join the radiative portion. The Hayashi phase is skipped entirely and the unrelaxed star first appears below the classical evolutionary track for that mass in the HR diagram. At this epoch, the star has a relatively shallow convection zone. During the subsequent relaxation phase, the stellar radius, surface luminosity and temperature all increase, while outer convection disappears. The luminosity in this mass range stems almost entirely from gravitational contraction;
- Stars more massive than $4M_{\odot}$ are *fully radiative stars*, and appear immediately on the radiative portion of the track, where they begin to contract homologously under their own gravity. As the star contracts, the average interior luminosity must rise as R_*^{-1} . This rise is evident in the evolutionary tracks of Fig. 2.1. The specific entropy decreases with time in all interior mass shells, a sign of homologous contraction. At any time, the interior is radiative, that is the entropy is increasing outward, except for a very thin surface layer. As already mentioned, stars with mass larger than $10M_{\odot}$, have not a pre-main-sequence phase, because they become optically visible after having ignited central hydrogen.

[†]A nearly vertical path of stellar evolution on the Hertzsprung-Russell diagram down which an infant star progresses on its way to the main sequence. While on the Hayashi track, a star is largely or completely in convective equilibrium; as it progresses, its luminosity, initially very high, decreases rapidly with contraction, but its surface temperature remains almost the same. The sequence runs in reverse for stars leaving the main sequence to become giants.

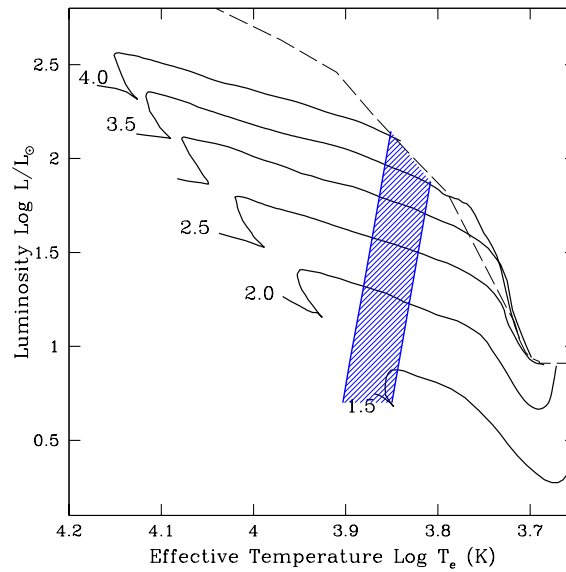


Figure 2.2: Evolutionary tracks for PMS stars together with the instability strip computed by Marconi & Palla(1998).

2.3 PMS δ Scuti stars

Pre-main sequence intermediate mass stars with mass in the range $1.5 < M/M_{\odot} < 4$ cross the pulsation instability strip during their contraction towards the main sequence as showed in Fig. 2.2.

The existence of pulsating stars among the PMS intermediate mass stars was originally suggested by Breger(1972), who identified the first two candidates, V588 Mon and V589 Mon in the young cluster NGC2264. About 20 years later, new empirical evidences for δ Scuti-like pulsation were found by Kurtz and Marang (1995) and Donati et al. (1997) for the Herbig Ae stars HR 5999 and HD 104237, respectively and many new members were identified in the following years(see next section).

Pulsation is manifested observationally through small, temporal variation of the stellar brightness as showed in figure 2.3. expected to be pulsating in a similar way as the MS and post-MS δ Scuti stars, that is with more than one period of oscillation due to both radial and non radial motion.

Pulsation arises in this PMS phase of stellar evolution by means of the classical κ mechanism. Depending on its mass, a given star shows intrinsic pulsation from 5 to 10 percent of its PMS lifetime. Thus, the potential number of candidate sources is

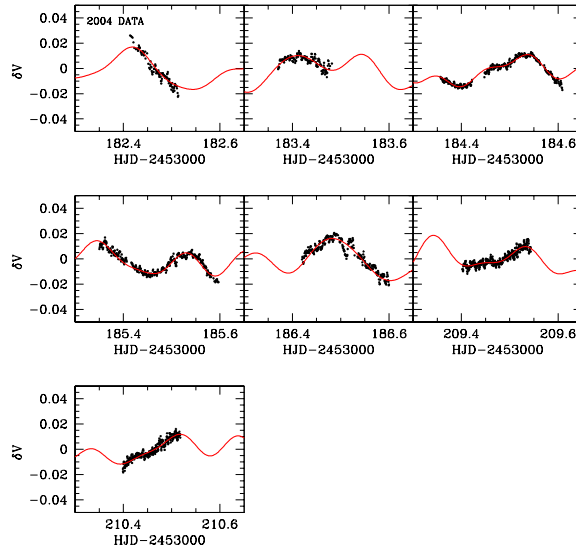


Figure 2.3: light curves for the δ Scuti PMS star VV Ser from Ripepi et al. 2006. Note that $\delta V = V_{VAR} - V_{COMP}$. The solid line displays the fit to the data with all the significant frequencies found for this star.

rather limited, and the actual number of known PMS δ Scuti stars is about 35. In the following section we describe observational results obtained for δ Scuti pulsations in intermediate mass PMS stars.

2.4 Present observational status

As mentioned above Breger(1972) was the first to report short-term photometric variation resembling δ Scuti pulsations in two PMS stars (V588 Mon, V589 Mon). Only monopercidities were detected, with considerable ambiguity on their reality and large uncertainties on their frequencies, due to the limited amount of data.

This initial finding was confirmed by subsequent observation of δ Scuti-like pulsations in other Herbig Ae stars. Recently the interest for this class of objects has significantly grown up and the actual number of known or suspected candidates amounts to about 35 (see Table 2.1).

In particular 29 of them have been studied photometrically, but most of them have insufficient data due both to the short duration of the observations and/or to the poor

duty cycle. It is very clear that data of much better quality are needed, in particular data spanning at least a couple of weeks, with improved duty cycles. Multisite campaigns and/or space-based observations are necessary to reach this goal. Up to now only 6 stars have been observed by means of multisite campaigns and all of them have been found to be multiperiodic: V588 and V589 Mon (12 and 19 frequencies respectively, Zwintz et al. 2005), V351 Ori (5 frequencies, Ripepi et al. 2003), IP Per (9 frequencies, Ripepi et al. 2006), HD 34282 (9 frequencies, Amado et al. 2005), and V346 Ori (17 frequencies, Ripepi et al. in preparation).

Spectroscopic monitoring of PMS stars can also provide information on their δ Scuti pulsations. Radial velocity curves can be used to study low-degree modes, with a sensitivity to the various modes which differs from that of photometric observations. Radial velocity curves therefore provide a tool of investigation for pulsations which is independent from and complementary to photometry, and can be used for instance to confirm the frequencies found in photometry. However, only for few stars spectroscopic monitoring has been carried out. In particular spectroscopic measurements are available for the following stars: V351 Ori (5 frequencies Balona et al. 2002), β Pic (19 frequencies Koen et al. 2003), HD 104237 (5 frequencies, Böhm et al. 2004), and the binary star RS Cha (Alecian et al. 2005, 2006). This last object is very interesting because it is an eclipsing double-line spectroscopic binary. Results based on high resolution spectroscopy (Alecian et al. 2006) seem to show that both components are pulsating. This star therefore will offer the unique opportunity to obtain stringent constraints on pulsating models.

Space-based observations are definitely the best strategy for asteroseismology, providing both a very good spectral window and a very low level of photometric noise. Among the ongoing asteroseismology space projects, CoRoT (for Convection, Rotation and planetary Transit) and MOST (Microvariability and Oscillation of STars) have the possibility of observing PMS stars as part of their programme.

CoRoT (Baglin et al., 2002) is a small space photometry space mission, for asteroseismology and exoplanet search. It is being developed by CNES, the french space agency, with a significant participation from other european countries, Brasil and ESA, and includes a 27 cm CCD photometer placed on the low-earth orbit, covering

a 3 degree field. It will be launched on December 2006 (hopefully). The duty cycle of the observations will be better than 96%, which also is by far more efficient than multisite ground based campaigns. CoRoT will observe a few fields for 5 months continuously, and also a few other fields for 10 - 20 days, in order to perform a seismological exploration of the HR diagram. There will be a possibility to observe a few PMS stars in this exploratory phase of the mission, in particular the young cluster NGC 2264, which falls in the continuous viewing zone instrument. This will give us the first opportunity to detect and measure low amplitude modes, with a good frequency resolution and most of all no alias.

MOST is a microsatellite desined to probe stars and extrasolar planets. MOST was lunched on June 30, 2003, and has as scientific goals the detection and the characterization of: 1) the acoustic oscillation in Sun-like stars, to probe seismically their structure and ages; 2) the reflected light from giant exoplanets closely orbiting Sun-Like stars, to reveal their size and atmospheric compositions; 3) turbulent variations in massive evolved stars to understand how they add gas to interstellar medium.

The experiments intends to performe ultra-high-precision photometry (i.e., measurement of brightness variation to a level od 1 part per million) of stars down to the magnitude 6 for up to months without interruptions. The instuments is equipped with an optical telescope with a collecting mirror only 15 cm across, with two CCD camera (1024X1042 pixels). One CCD is used for science measurements; the other is read out every second to track guide stars for satellite altitude control. The instrument has a single broadband filter which selects in light the wavelengh range between 350 to 700nm. MOST has already observed the two prototypes of the class: V588 and V589 Mon. The results will be avaiable in the near future.

2.5 Present theoretical status

The observational campaigns performed by Kurutz & Marang (1995), Donati et al. (1997), which confirmed the δ Scuti like pulsations in the Herbig Ae stars HR5999 and HD104237 respectively, stimulated the first theoretical investigation of pulsation properties of the PMS intermediate mass stars. Marconi & Palla (1998) cal-

culated the topology of the PMS instability strip for the first three radial modes, based on non-linear convective hydrodynamical models (see Fig. 2.2). These authors also pointed out that the interior structure of PMS stars entering the instability strip differs significantly from that of more evolved Main Sequence stars (with the same mass and temperature), even though the envelopes structures are similar. This property was subsequently confirmed by Suran et al. (2001) who made a comparative study of the seismology of a $1.8 M_{\odot}$ PMS and post-MS star. Suran et al. found that the unstable frequency range is roughly the same for PMS and post-MS stars, but that non radial modes are very sensitive to the deep internal structure of the star. In particular, it is possible to discriminate between the PMS and post-MS stage, using differences in the oscillation frequency distribution in the low frequency range (g modes). Recently Grigahcène et al. (2006) have determined a theoretical PMS instability strip obtained for the first seventh radial overtones, by performing non-adiabatic convective pulsations calculations.

However not all the observed frequencies can be interpreted as radial modes, but some of that seems to be non radial oscillation frequencies. A systematic study of non radial oscillation has not been performed yet. In this work we have planned to investigate the pulsation properties of intermediate PMS stars by means of both radial and non radial models. To this purpose we have built a fine grid of PMS models with mass ranging from 1.6 to $4 M_{\odot}$, for which we have computed the radial and non radial pulsation behaviour. The theoretical tools used in this thesis will be described in the next chapter.

Table 2.1: Pulsating PMS stars.

Name	Spectral Type	V	\log_{eff}	$\log L/L_{\odot}$	Type	number of freq.
V589 Mon	F2 III	3.85	1.51	CM		19
V588 Mon	A7 III/IV	3.9	2.05	CM		12
NGC 6823 HP57	-	3.86	1.25	CM		2
NGC 6823 BL50	-	3.86	1.6	CM		2
NGC 6383 198	-	3.87	1.3	CM		1
NGC 6383 170	A5 IIIp	3.91	1.7	CM		5
IC 4996 40	A4	3.93	1.26	CM		1
IC 4996 37	A5	3.91	1.26	CM		1
IC 348 H 254	F0(A8 III-IV)	3.85	1.62	CM		4
NGC 6530 5	-	3.92	1.2	CM		2
NGC 6530 82	-	3.88	1.01	CM3		
NGC 6530 85	A1 III	3.86	1.37	CM		5
NGC 6530 263	-	3.87	1.13	CM		1
NGC 6530 278	A0/A5	3.9	1.75	CM		9
NGC 6530 281	-	3.92	1.29	CM		7
V351 Ori	A7 IIIe	3.87	1.15	HAEBE		5
V346 Ori	A5 III	3.89	0.98	HAEBE		4
UX Ori	A3e	3.94	1.49	HAEBE	suspected	
IP Per	A7 V	3.89	0.97	HAEBE		9
HR 5999	A7 III/IVe	3.85	2.12	HAEBE		1
HD 35929	F0 IIIe	3.86	1.92	PMS?		1
HD 142666	A8 Ve	3.88	1.03	HAEBE		1
HD 104237	F4 V	3.93	1.5	HAEBE		2(3?)
CQ Tau	F2 IVe	-	-	HAEBE		1
BF Ori	A5II-IIevar	3.83	1.48	HAEBE		1(?)
HD 34282	A0e	3.94	1.15	HAEBE		2
V1247 Ori	A5 III	3.86	1.2	PMS?		1
β Pic	A5V	3.91	1.05	PMS?		2(3?)
VV Ser	A2e	3.85	2.13	HAEBE		2(3?)
V375 Lac	A7e	3.86	2.08	HAEBE		2
WW Vul	A3e	-	-	HAEBE		1(1?)
PX Vul	F0Ve	-	-	HAEBE		1(?)

Theoretical tools to reproduce PMS δ Scuti pulsation

In this section I present the theoretical tools used in this thesis to characterize the pulsational properties of pre-main-sequence δ Scuti stars. In particular I describe the evolutionary and pulsational codes. At the end of the chapter, the theoretical frequencies are presented and a first application to an observed pulsator, namely the Herbig star VV Ser is discussed.

3.1 Evolutionary models

The first step to analyze the pulsation properties of PMS δ Scuti stars, is to build a set of PMS evolutionary models, from which the equilibrium stellar structures, that are the input of any pulsational code, are obtained.

The stellar models used in this thesis have been computed with the CESAM evolutionary code (Morel, 1997) including update physical assumptions (Marques et al., 2006) and optimized for asteroseismologic purposes. The precise calculation of the oscillation frequencies of both p and g modes, requires numerically precise and

adequately dense mesh distributions in the evaluation of the quantities describing the internal structure and entering the oscillation equations. The PMS models are obtained by solving the classical equations of stellar structure, (see 1.13 - 1.16). In the CESAM code the independent lagrangian variable is the mass M_r in a sphere of radius r . The star is assumed as a spherical symmetric object, without magnetic field, and with rotation, so the equations of the stellar structure are written as:

$$\frac{\partial P}{\partial M} = -\frac{GM}{4\pi R^4} + \frac{\Omega^2}{6\pi R} \quad (3.1)$$

for the hydrostatic equilibrium, where $\Omega(M, t)$ is the angular velocity.

$$\frac{\partial T}{\partial M} = \frac{\partial P}{\partial M} \frac{T}{P} \nabla \quad (3.2)$$

for the thermal balance, where $\nabla = \frac{\partial \ln T}{\partial \ln P}$.

$$\frac{\partial R}{\partial M} = \frac{1}{4\pi R^2 \rho} \quad (3.3)$$

for the continuity equation.

$$\frac{\partial L}{\partial M} = \epsilon - \frac{\partial U}{\partial t} + \frac{P}{\rho^2} \frac{\partial \rho}{\partial t} \quad (3.4)$$

for the energy equation and,

$$\frac{\partial X_i}{\partial t} = -\frac{\partial F_i}{\partial M} + \Psi_i \quad , 1 \leq i \leq n_X \quad (3.5)$$

for the changing in chemical composition, where $X_i(M, T)$ is the fraction of unit mass which consist of nuclei of type i , F_i the flow of X_i due to diffusion, Ψ_i the creation rate of X_i due to thermonuclear reactions, and n_X the number of chemical species.

The physical and numerical properties of these models are discussed in detail in the paper by Morel (1997). The main characteristics can be summarized as follows:

- the evolution is initialised with an homogeneous, fully convective model in quasi-static contraction, with a central temperature inferior to the ignition temperature of deuterium;

- the OPAL equation of state (Rogers et al. 1996, 2001) and the opacities by Iglesias & Rogers (1996), complemented, at low temperatures, by the Alexander & Ferguson (1994) molecular opacities, are adopted;
- the temperature gradient in the superadiabatic convective zones is computed using the standard mixing-length theory (Böhm-Vitense 1958) with $l/H_P = 1.6$.

For the frequencies, the computation of the following variables is needed at each mesh point in the model:

$$\begin{aligned}
 x &= \frac{r}{R} \\
 a_1 &= \frac{q}{x^3} \quad \text{where } q = \frac{m}{M} \\
 a_2 &= \frac{-1}{\Gamma_1} \frac{d \ln P}{d \ln r} = \frac{Gm\rho}{\Gamma_1 p r} \\
 a_3 &= \Gamma_1 \\
 a_4 &= \frac{-1}{\Gamma_1} \frac{d \ln P}{d \ln r} - \frac{d \ln \rho}{d \ln r} \\
 a_5 &= \frac{4\pi\rho r^3}{m}
 \end{aligned} \tag{3.6}$$

These are clearly all dimensionless. The relations between the variable defined here and more “physical” variables used in the differential system equation are:

$$\begin{aligned}
 p &= \frac{GM^2}{4\pi R^4} \frac{x^2 a_1^2 a_5}{a_2 a_3} \\
 \frac{dp}{dr} &= \frac{-GM^2}{4\pi R^5} x a_1^2 a_5 \\
 \rho &= \frac{M}{4\pi R^3} a_1 a_5
 \end{aligned} \tag{3.7}$$

The Lamb frequency S_l and the buoyancy frequency, S_l , are written as:

$$S_l^2 = \frac{l(l+1)c^2}{r^2} = \frac{GM}{R^3} \frac{l(l+1)a_1}{a_2} \tag{3.8}$$

and

$$N^2 = \frac{GM}{R^3} a_1 a_4 \tag{3.9}$$

In addition the following “global” quantities are used in the frequencies computations code.

$$\begin{aligned}
 D_1 &= M_* \\
 D_2 &= R_* \\
 D_3 &= p_c \\
 D_4 &= \rho_c \\
 D_5 &= -\left(\frac{1}{\Gamma_1 p} \frac{d^2 p}{dx^2}\right)_c \\
 D_6 &= -\left(\frac{1}{\rho} \frac{d^2 \rho}{dx^2}\right)_c \\
 D_7 &= \mu
 \end{aligned} \tag{3.10}$$

Here R and M are the photospheric radius and mass of the model (the photosphere being defined as the point where the temperature equals the effective temperature). In a complete model p_c and ρ_c are the central pressure and density, and D_5 and D_6 are evaluated at the centre. In an envelope model D_3 and D_4 should be set to the values of pressure and density at the innermost mesh point and D_5 and D_6 may be set to zero.

On this basis we have computed 56 models for stellar masses varying from 1.6 to $4M_\odot$ with a step of $0.2M_\odot$. The evolutionary tracks are shown in figure Fig. 3.1, while the physical properties of the selected PMS models are reported in Table 3.1.

3.2 Pulsational approach

The linear adiabatic non radial oscillations are described completely by the set of differential equations derived in chapter one (see Eqs. 1.33 - 1.37). The numerical code I have used for solving those equations calculation is the linear and adiabatic “Aarhus” code named ADIPS (<http://astro.phys.au.dk/~jcd/adipack.n/>) built ad “hoc” for the Sun, and adapted in this thesis to PMS δ Scuti stars. The code has been applied to the PMS stellar equilibrium models described in the previous

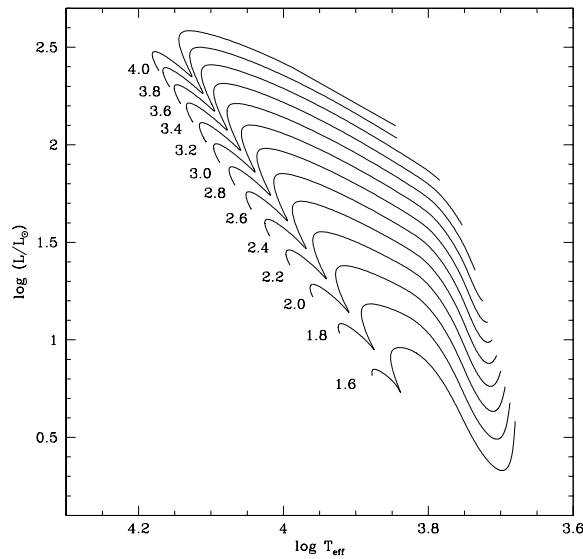


Figure 3.1: PMS evolutionary tracks computed with the CESAM code for the labelled stellar masses (in M_{\odot} .)

section.

The general oscillations equations appear quite complicate. In particular, analytical solutions can only be obtained in certain, very restricted cases. However the understanding of the numerical results and the interpretation of the observed oscillations have been greatly assisted by asymptotic analyses of the oscillation equations. In the next section I present the asymptotic properties of the oscillation equations and then the numerical techniques commonly adopted to obtain the solutions.

3.3 Asymptotic theory

The general equations are of fourth order. This is a difficulty in asymptotic studies which generally deal with second-order systems. Luckily enough, the perturbation to the gravitational potential, Φ' , can be neglected when the harmonic (l) or radial ($|n|$) degree is large. This approximation was first studied carefully by Cowling (1941), and is therefore known as the *Cowling approximation*. It reduces the order of the system of equations to the second, with a corresponding reduction in the number of boundary conditions. The two equations in the Cowling approximation

can be combined into a single second-order differential equations for the radial component of displacement perturbation, ξ_r :

$$\frac{d^2\xi_r}{dr^2} = \frac{\omega^2}{c^2} \left(1 - \frac{N^2}{\omega^2}\right) \left(\frac{S_l^2}{\omega^2} - 1\right) \xi_r \quad (3.11)$$

This equation represents the crudest possible approximation to the equations of non-radial oscillations.

From equation 3.11, it is clear that the characteristic frequencies S_l and N , play a very important role in determining the behaviour of the oscillations. To analyze the properties of oscillations it is convenient to write equation 3.11 as:

$$\frac{d^2\xi_r}{dr^2} = -K(r)\xi_r \quad (3.12)$$

where $K(r) = \frac{\omega^2}{c^2} \left(1 - \frac{N^2}{\omega^2}\right) \left(\frac{S_l^2}{\omega^2} - 1\right)$. The local behaviour of ξ_r depend on the sign of $K(r)$. Where $K(r)$ is positive, ξ_r is locally an oscillation function of r ; where $K(r)$ is negative the solution is locally an exponentially increasing or decreasing function of r . Thus according to this description the solution oscillates when:

- $|\omega| > |N|$ and $|\omega| > S_l$, (*p* mode);
- $|\omega| < |N|$ and $|\omega| < S_l$, (*g* mode).

and it is exponential when:

- $|N| < |\omega| < S_l$,
- $S_l < |\omega| < |N|$

For a given mode of oscillation there may be several regions where the solution oscillates, with intervening regions where it is exponential. However, in general, one of these oscillating regions is dominant. The solution is then said to be *trapped* in this region; its frequencies are predominantly determined by the structure of the model in the region of trapping. There are two distinct type of trapping regions. The *p* type region extends from a point in the interior to just below the surface. Modes corresponding to this type of trapping are the *p* modes and typically occurs at high frequencies. The *g* type region is a region in the interior and modes corresponding to this trapping are the *g* modes, typically occurring at low frequencies. From the

asymptotic theory derives that for $n \gg l$ the p modes have a very regular pattern:

$$\nu_{nl} \simeq \Delta\nu[n + (1/2)l + \epsilon] + \frac{1}{6}Al(l + 1) \quad (3.13)$$

where A , $\Delta\nu$ and ϵ are constants (Tassoul 1980, Gough 1986). The last term is a rather small correction compared to the first one. It is evident that modes with the same l and with adjacent values of n are separated by $\Delta\nu$, and that frequencies of modes with degree l and order n , and degree $l+2$ and order $n-1$ differ by the small amount $(2l+3)A/3$. The term $\Delta\nu$ is asymptotically given by: $\Delta = (2 \int_0^{R_*} \frac{dr}{c})$, where c is the local sound speed and R_* is the stellar radius. Then, it is possible to define the large frequency separation as:

$$\Delta\nu_l \equiv \nu_{nl} - \nu_{n-1l} \quad (3.14)$$

between modes of the same order, and the small frequency separation as:

$$\delta_{ll+2} \equiv \nu_{nl} - \nu_{n-1l+2} \quad (3.15)$$

between modes whose degrees differ by two. The small separation is sensitive to the sound speed gradients, particularly in the stellar core. In detail the small separation is given by $\delta_{ll+2} = \Delta\nu_l \frac{(l+1)}{2\pi^2\nu_{nl}} \int_0^{R_*} \frac{dc}{dr} \frac{dr}{r}$.

In the asymptotic limit $n \gg l$, g -mode periods become almost equally spaced:

$$T_{nl} = \frac{T_0(n + l/2 + \delta)}{L} \quad (3.16)$$

where T_{nl} is the period of a g -mode, T_0 and δ are parameters.

3.4 Numerical Techniques

The differential equations 1.33 - 1.37, in combination with the boundary conditions, constitute a two-point value problem. Nontrivial solutions to the problem can be obtained only at selected values of the frequency ω , which is therefore an eigenvalue of the problem. Here I describe the general properties of the solution methods.

3.4.1 Difference Equations

The numerical problem can be formulated generally as that of solving:

$$\frac{dy_i}{dx} = \sum_{j=1}^I a_{ij}(x)y_j(x) \text{ for } i=1, \dots, I \quad (3.17)$$

with suitable boundary conditions at $x = x_1$ and x_2 . Here the order I of the system is 4 for the full nonradial case, and 2 for radial oscillations or the Cowling approximation.

To handle these equations numerically, it is useful to introduce a mesh $x_1 = x^{(1)} < x^{(2)} < \dots < x^{(N_{me})} = x_2$, in x where N_{me} is the total number of mesh points. Similarly, they are defined $y_i^{(n)} = y_i(x^{(n)})$, and $a_{ij}^{(n)} = a_{ij}(x^{(n)})$. A very simple representation of the differential equations is in term of *second-order centred differences*, where the differential equations are replaced by the difference equations:

$$\frac{y_i^{(n+1)} - y_i^{(n)}}{x_i^{(n+1)} - x_i^{(n)}} = \frac{1}{2} \sum_{j=1}^I [a_{ij}^{(n)} y_j^{(n)} + a_{ij}^{(n+1)} y_j^{(n+1)}] \quad i=1, \dots, I \quad (3.18)$$

These equations allow the solution at $x = x^{(n+1)}$ to be determined from the solution at $x = x^{(n)}$.

Alternatively, it is possible to approximate the differential equations at each mesh interval $(x^{(n)}, x^{(n+1)})$ with a set of equations with constant coefficients, as given by:

$$\frac{dy_i^{(n)}}{dx} = \sum_{j=1}^I \tilde{a}_{ij}^n y_j^{(n)}(x) \quad \text{for } i=1, \dots, I \quad (3.19)$$

where $\tilde{a}_{ij}^n = \frac{1}{2}(a_{ij}^n + a_{ij}^{n+1})$ (Grabriel & Noels 1976). These equations may be solved analytically on the mesh interval, and complete solutions are obtained by continuous matching at the mesh points. This technique becomes very complex for four order systems, so it is implemented only for systems of order 2, i.e., radial oscillations or non-radial oscillations in the Cowling approximation. The adopted code allow us to solve the equation system with two basically different techniques. The first is a shooting method, where solutions satisfying the boundary conditions are integrated separately from the inner and outer boundary, and the eigenvalue is found by matching these solutions at a suitable inner fitting point. The second is the relaxation technique, that solve the equations, together with a normalization

condition and then found by requiring the continuity of one of the eigenfunctions at an interior matching point when all the boundary conditions are satisfied, or by requiring that the remaining boundary condition be satisfied.

The physical and numerical assumptions used in this thesis for the computation of pulsation frequencies are:

- The lagrangian perturbation of the pressure is set to zero;
- The equation are solved by means of the shooting method with the standard second-order centered difference technique;
- The frequencies are corrected for truncation errors through the Richardson extrapolation.

3.5 The predicted pulsational frequencies:the case of VV Ser

In order to explore the pulsation frequencies that characterize the PMS stars, associated to both radial and non radial modes, I have applied the Aarhus adiabatic non-radial pulsation code to 56 models for stellar masses varying from 1.6 to 4.0 M_{\odot} with a step of 0.2 M_{\odot} (see table 3.1). For each selected mass, I have considered from two to four different effective temperatures in the range 6000 to 10000 K , along the corresponding evolutionary tracks. These PMS models cover the HR diagram location expected for pulsating PMS intermediate mass stars. For each models I have computed the frequencies for p and g modes for $l = 0, 1, 2$ and $|n| = 0$ to 20. I have analyzed only the mode with $l = 0, 1, 2$. In fact as underlined by Suran et al. 2001, Baglin et al. 2000 they are thought to be the easiest to detect, as their visibility coefficients remain sufficiently large after integration over the whole stellar disk.

In fig. 3.2 I report the predicted frequencies for the models at 3.2 and 3.6 M_{\odot} , as a function of the radial degree n . As shown in the figure, the range covered by the predicted p and g mode frequencies depends on both the stellar mass and the

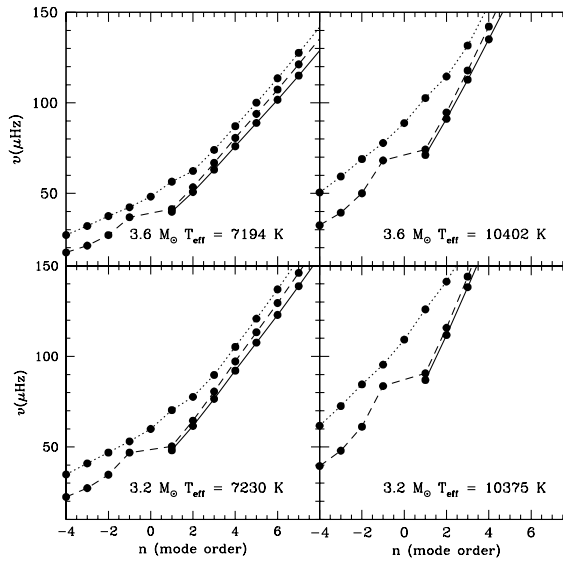


Figure 3.2: Predicted frequencies as function of the radial order n for models at $3.2 M_{\odot}$ (bottom panel), and $3.6 M_{\odot}$ (upper panel). Symbols are connected by a full line in the case $l = 0$, by dashed line for $l = 1$ and by dotted line for $l = 2$. The effective temperatures of the models are indicated for each mass.

effective temperature, moving toward higher values as the stellar mass decreases, at fixed effective temperature, and as the effective temperature increases, at fixed stellar mass.

As a first application we compare the PMS theoretical frequencies with the observed ones for the star VV Ser.

The variable VV Ser was defined as a young star in the seminal work by Herbig (1960) on emission line stars associated with reflection nebulae. The star is located in the Serpens molecular cloud (Chavarría et al. 1988) and has been widely studied in the literature. Although its properties and position in the HR diagram are still rather uncertain, the physical properties of this star as reported in literature are reported in table 3.2 .

VV Ser has been observed, by my group, in several runs during 2002, 2003 and 2004, using the Loiano 1.5m telescope. All the data have been reduced following the usual procedures (de-biasing, flat-fielding) by using standard IRAF routines.

On the basis of our analysis VV Ser is classified as a multiperiodic pulsator and the computed frequencies are reported in 3.3. In order to compare the observations

with the theoretical predictions, it is necessary to estimate the position of VV Ser in the HR diagram. For determining the T_{eff} value it is possible to use the spectral type and the table which convert it in effective temperature. In table 3.4, I report (first column) all the independent measurements of spectral type (ST) found in the literature. There is still a large uncertainty on the ST with values varying from B1e-B3e to A3e. The determination of the earliest types by [25] is based on the HeI 5876 Å line which was later found to be associated with the hot regions of accretion disks (see [61] and references therein) and therefore should not be considered reliable. However, a Be type has been found by several authors (see Table 3.4), ranging from B5 to B9. On the other hand, Table 3.4 lists six studies where VV Ser is classified as an Ae star, with typical ST A2. Interestingly, the only paper exclusively dedicated to VV Ser is that by [14], who assigns an A2e class, based on high resolution spectroscopy and Strömgren photometry. In this work I rely on these last results, allowing an uncertainty of two subclasses to take into account the spread of spectral types found in the literature. Adopting this spectral type range, and using the [64] conversion tables, the range of allowed effective temperature is from 8000 to 10000K. For evaluating the luminosity it is necessary to have a good distance of the star. The distance estimate of VV Ser is related to that of the Serpens Cloud, that in turn is still matter of debate. In fact, [14] and [19], on the basis of photometric and spectroscopic observations of 5 stars in the cloud (excluding VV Ser) calculated a distance of $D=311\pm 38$ pc, in fair agreement with previous determinations of about 440 pc by [56] and [69]. However, since such large distances to the Serpens cloud appear unlikely, in the following we will adopt a distance of 300-400 pc.

Concerning the luminosity, I simply decided to investigate all the luminosities in the range $1.3 < \log L/L_{\odot} < 2.3$, covering the empirical estimates in the literature (see 3.4).

On this basis I have analyzed all the region showed in figure 3.3, as the large box in the HR diagram. In particular I have selected all the PMS models in that region, that are represented as points on the evolutionary tracks. The figure also includes the theoretical instability strip computed for the first three radial modes by Marconi

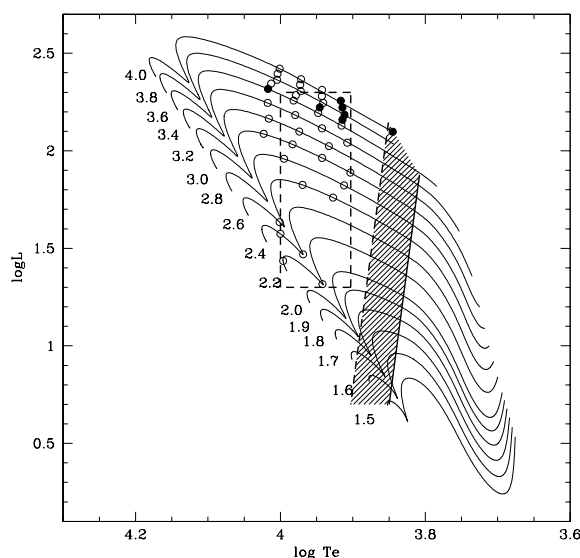


Figure 3.3: PMS evolutionary tracks for the labelled masses and solar chemical composition ($Z = 0.02$, $Y = 0.28$) computed with the CESAM code as compared with the estimated uncertainties on the position of VV Ser (dashed box, see text) and the theoretical instability strip for the first three radial modes predicted by [43] on the basis of nonlinear convective pulsation models. The empty circles represent the 32 models run for the pulsational analysis. The filled symbols are for the best fit models.

& Palla 1998, on the basis of nonlinear convective pulsation models. From this plot it is possible to see that for the estimated VV Ser effective temperatures it is not allowed pulsation in the first three radial modes, because the predicted instability strip is cooler at each luminosity level. However, we can expect pulsation in higher radial overtones and/or in nonradial modes.

In order to compare the theoretical frequencies with the observed ones I have plotted in Fig. 3.4 the predicted frequencies with $l = 0, 1, 2$ as a function of the mode order n ; the observed frequencies are represented by the horizontal lines.

As it is shown by these plots, the three lowest frequencies, namely f_2 , f_3 and f_4 , cannot be reproduced simultaneously by p modes, in the mass and effective temperature range found in literature. In particular, f_2 is only consistent with a g mode unless the effective temperature is much lower than the estimated empirical range. At this purpose I plot in Fig. 3.5, the comparison between theoretical and observed

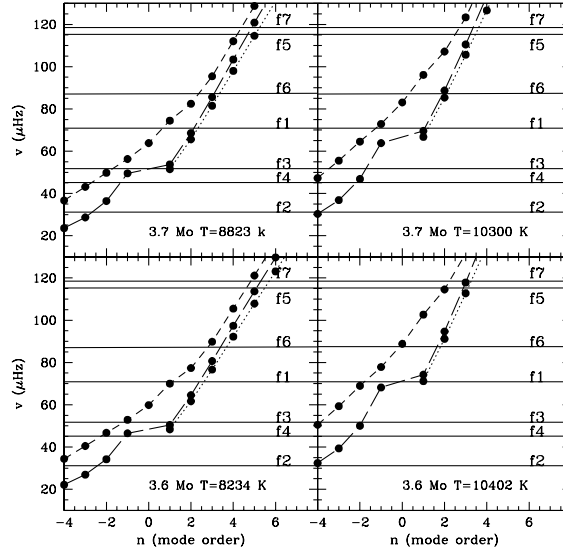


Figure 3.4: Comparison between predicted (filled symbols) and observed (horizontal solid lines) periodicities for models at $3.6 M_{\odot}$ (bottom panels), and $3.7 M_{\odot}$ (upper panels). Symbols are connected by a dotted line in the case of $l=0$, by a long dashed line for $l=1$ and by a dashed line for $l=2$. The two panels refer to the labelled effective temperatures. When a predicted frequency reproduces an observed one the corresponding filled symbol (along the given l slanting line) is located at the intersection with the horizontal line representing the observed value

frequencies for a significantly cooler model ($T_{eff} = 6997K$) with mass $M = 4M_{\odot}$. In this case, the range of the lowest observed frequencies is covered with the predicted $l = 0, n = 0, 1, 2$ modes, with f_2 close to the theoretical result for the fundamental mode. In other words at such low effective temperature it is possible to have pulsation in the lowest three radial modes, as predicted by the instability strip computed by Marconi & Palla(1998) (see Fig.3.3).

A tentative mode identification based on the various plots is summarized in Table 3.5. Model frequencies are required to match the observed ones within $2.5\mu Hz$, in order to take into account both the mean error on the measured periodicities ($\sim 0.5\mu Hz$) and an estimate of the (unknown) model intrinsic uncertainty.

Table 3.5: (continued)

Model			f_1	f_2	f_3	f_4	f_5	f_6	f_7
Mass	T_{eff}	l	Possible value of n						
4.0	9 366	1				-1	5		5
		2	1	-5	-1	-2			
mod41		0	2					3	
4.0	10 023	1		-3	-1				
		2	0	-6	-2	-3		2	4

The models reproducing all the observed frequencies with $l=0,1,2$ p and/or g (or f) modes are the ones reported in Table 3.6 and shown in Fig. 3.5 as filled circles.

Among these best fit models I have included the cooler ones (mod37). In this case all the seven observed frequencies can indeed be reproduced by p modes. Therefore, I found that either the effective temperature reported in the literature is significantly overestimated, or that it is possible to have pulsation in at least one g mode. This possibility is allowed, available studies point towards the existence of unstable low degree p -modes in PMS δ Scuti stars. Therefore, in my analysis, models with p -modes in the observed frequency range have been preferred. The possibility that g modes are also excited to the observed amplitudes has still to be confirmed. The stellar masses and luminosities associated with this models range from 3.6 to $4.0M_{\odot}$ and $\log L/L_{\odot} \approx 2.1-2.3$ respectively. This degeneracy could be removed, if another physical observable is known. This could be the large separation between the frequencies. In the next chapter I discuss a methodology built for reproducing the observed frequencies on the basis of the knowledge of the large frequency separation.

Table 3.1: Physical properties of the selected pre-main sequences models.

Model	Mass M/M _⊙	Radius R/R _⊙	Luminosity L/L _⊙	T _{eff} K	Age Gy
mod1	1.6	1.78	7.18	7078	11.21
mod2	1.6	1.52	6.72	7548	16.82
mod3	1.8	2.32	15.23	7493	7.86
mod4	1.8	1.78	9.70	7648	9.83
mod5	1.8	1.61	11.59	8401	11.80
mod6	2.0	1.88	14.27	8184	7.41
mod7	2.0	1.70	18.40	9186	8.89
mod8	2.2	3.67	18.70	6273	4.07
mod9	2.2	3.10	30.04	7681	4.66
mod10	2.2	1.99	20.74	8749	5.82
mod11	2.2	1.77	27.27	9913	6.98
mod12	2.4	4.14	24.06	6288	3.25
mod13	2.4	3.48	39.04	7739	3.72
mod14	2.4	2.09	29.46	9304	4.65
mod15	2.4	2.04	37.54	10000	5.11
mod16	2.6	4.55	33.38	6506	2.82
mod17	2.6	3.92	48.15	7688	3.10
mod18	2.6	3.54	57.56	8459	3.24
mod19	2.6	3.14	66.90	9319	3.38
mod20	2.6	2.18	43.08	10023	4.09
mod21	2.8	4.81	46.39	6876	2.40
mod22	2.8	4.46	55.53	7468	2.51
mod23	2.8	4.08	66.50	8168	2.63
mod24	2.8	3.23	90.99	9885	2.85
mod25	3.0	5.58	46.31	6381	1.90
mod26	3.0	4.96	64.92	7366	2.08
mod27	3.0	4.17	91.89	8758	2.26
mod28	3.0	3.74	107.9	9621	2.35
mod30	3.0	3.32	122.2	10547	2.45
mod31	3.2	6.13	53.10	6301	1.57
mod32	3.2	5.49	74.04	7230	1.73
mod33	3.2	4.67	105.7	8573	1.88
mod34	3.2	4.22	125.5	9417	1.96
mod35	3.2	3.75	146.2	10375	2.04
mod36	3.4	6.46	69.66	6567	1.37
mod37	3.4	5.76	94.50	7502	1.49
mod38	3.4	4.96	130.4	8762	1.61
mod39	3.4	4.53	152.5	9539	1.67
mod40	3.4	4.08	176.0	10414	1.73
mod41	3.6	7.29	67.80	6139	1.09
mod42	3.6	6.46	100.3	7194	1.24
mod43	3.6	5.71	134.7	8234	1.33
mod44	3.6	4.88	180.9	9590	1.43
mod45	3.6	4.44	207.6	10402	1.48
mod46	3.8	7.84	81.15	6194	0.94
mod47	3.8	6.94	116.3	7203	1.06
mod48	3.8	6.21	152.9	8155	1.14
mod49	3.8	5.40	202.2	9376	1.22
mod50	3.8	4.97	231.2	10106	1.26
mod52	4.0	8.25	101.0	6375	0.83
mod53	4.0	7.30	140.7	7369	0.92
mod54	4.0	6.58	180.5	8253	0.98
mod55	4.0	5.80	232.9	9366	1.05
mod56	4.0	5.40	263.8	10023	1.08

Table 3.2: Stellar parameters for VV Ser found in the literature.

V	D	A_V	$\log(T_{\text{eff}})$	$\log(L)$	M	source
mag	pc	mag	K	L_{\odot}	M_{\odot}	
12.666	245	6.1	3.95	> 1.62		1
11.87	440	3.0	4.03	1.8	3.3	2
11.92	440	3.4	4.14	2.23	3.8	3
11.63	296	3.4	3.95	1.51	2.1	4
11.58	440		4.03	2.03		5
	330	2.7	3.95	1.27		6

1=[14];

2=[37];

3=[36]; 4=[61];

5=[74];

6=[2]

Table 3.3: Computed VVSer pulsation frequency.

Frequency	error
(μHz)	(μHz)
f_1	70.8 \sim 0.5
f_2	31.1 \sim 0.5
f_3	51.7 \sim 0.5
f_4	45.1 \sim 0.5
f_5	115.2 \sim 0.5
f_6	87.5 \sim 0.5
f_7	120 \sim 0.5

Table 3.4: Literature values of Spectral Type, Luminosity Class for VV Ser.

Sp. Type	Source
A2e	Herbig (1960)
A:	[17]
B1e-B3e	[25]
A2eV β	[14]
B9e ¹	[37]
B5e	[24]
A3IIe β	[27]
A0V ϵ p ²	[49]
B+sh	[77]
A2IIIe ³	[2]
B6e	[36]

¹=photometrically determined

²=the Authors quote an error of five classes

³=the Authors quote van den Ancker (private communication) as source for this value

Table 3.6: Preliminary mode identification as a function of the explored model input parameters for models reproducing all the seven observed frequencies. The mass is in solar units (M_{\odot}) and effective temperature is in K.

Model		l	f_1	f_2	f_3	f_4	f_5	f_6	f_7	
Mass	T_{eff}		Possible value of n							
mod24	3.6	10 402	0	1						
			1		-4	-2				2
			2	-2	-8	-4	-5	2	0	
mod25	3.7	8 211	0	3		1	6	4	6	
			1		-2	-1				
			2	2	-4	-1	-2	5	3	
mod26	3.7	8 823	0			1	5			
			1	1	-3	-1		2	5	
			2		-5	-2	-3			
mod29	3.8	8 155	0	3		1				
			1	2	-2		6	4	6	
			2	2	-4	0	-1			
mod33	3.9	8 210	0			2				
			1	2	-2		6	4		
			2		-4	0	-1		6	
mod37	4.0	6 997	0	5	1	3	9		9	
			1			1		6		
			2	4	-2	2	1	8		8
mod38	4.0	8 253	0			2			7	
			1	2						
			2		-3	0	-1	6	4	6

A theoretical approach for the interpretation of pulsating PMS intermediate-mass stars

In this chapter I present a theoretical approach for the interpretation of pulsating PMS intermediate mass stars.

In the previous chapter I have described the theoretical tools used in this work and analyzed the asymptotic theory of g and p modes. I have also shown the behaviour of these modes as function of mass and effective temperature. The comparison between theoretical and observed periodicities has been found to be not sufficient to constrain the physical parameters of the star such as its mass and effective temperature. In the following sections it is verified the possibility of using the asymptotic theory for PMS intermediate mass stars, and it is shown a methodology that allow us to constrain the stellar parameters.

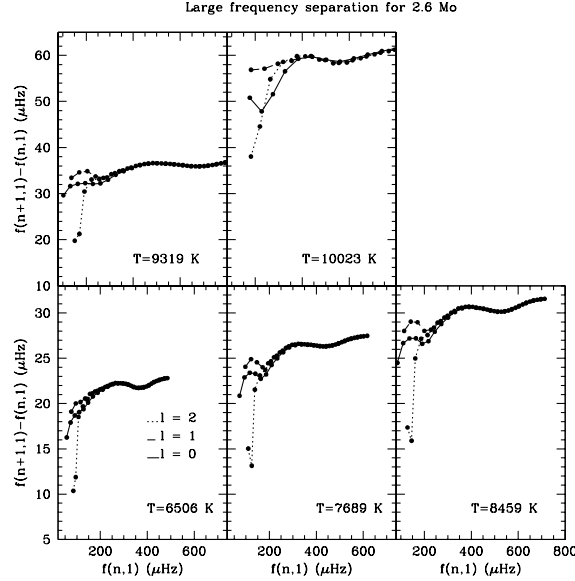


Figure 4.1: Large frequency separation as a function of the frequency for models with $M = 2.6M_{\odot}$ the labelled effective temperatures, for $1 < n \leq 20$. Symbols are connected by a full line in the case of $l=0$, by a dashed line for $l=1$ and by a dotted line for $l=2$.

4.1 Large frequency separation

As mentioned in Section 3.3, in the asymptotic regime the p -mode frequencies have a regular pattern, given by:

$$\nu_{n,l} \simeq \Delta\nu[n + l/2 + \epsilon] + \frac{A}{6}l(l+1) \quad (4.1)$$

where $\Delta = 2 \int_0^{R_*} \frac{dr}{c} \propto (\frac{M_*}{R_*})^{1/2}$. On this basis, it is possible to define the large frequency separation as:

$$\Delta\nu_{n,l} = \nu_{n,l} - \nu_{n-1,l} \sim \Delta\nu \quad (4.2)$$

The equation 4.1, and 4.2 imply that a relation between the large frequency separation, mass and radius can be found. In particular it is possible to link the large separation to the effective temperature and luminosity. In fact the radius is related to the effective temperature and the mass to the luminosity for each effective temperature. For this purpose I have computed the large frequencies separation for all the models reported in Table 3.1 with $l = 0, 1, 2$ and $0 \leq n \leq 20$.

In figure 4.1, I show for the models at $2.6M_{\odot}$, and the labelled effective temperatures, the behaviour of large separation, for $l = 0, 1, 2$, versus the frequency. By

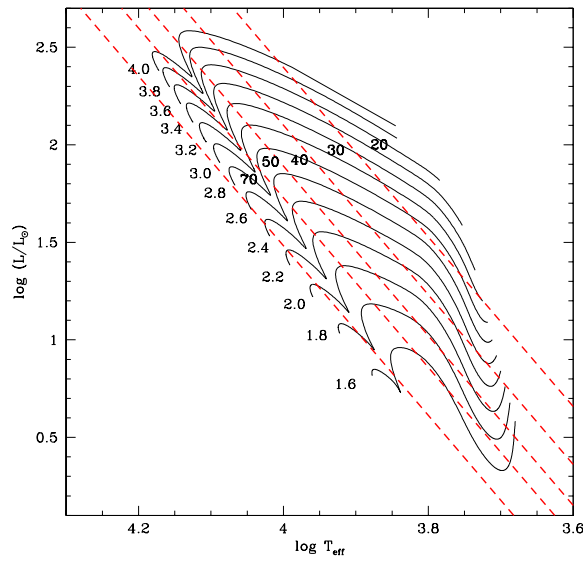


Figure 4.2: The linear fit given in eq. (4.3) is represented in the HR diagram by dashed lines, defined for a constant value of $\Delta\nu$ (as labelled, in μHz), from $20 \mu Hz$ to $70 \mu Hz$.

analyzing this plot I have verified that for low n values the asymptotic regime is not verified, but the large separation tends to a constant value for n larger than 5.

For deriving a relation between the large frequency separation, the effective temperature and the luminosity, I have considered the mean of all the $\Delta\nu$ values for $5 < n \leq 20$. Then I have obtained a linear logarithmic fit through my grid of models, as following:

$$\log L = (-12.81 \pm 0.02) + (4.35 \pm 0.05) \log T_{eff} - (1.681 \pm 0.0015) \log \Delta\nu \quad (4.3)$$

This fit is plotted in fig. 4.2, for selected values of $\Delta\nu$, ranging from $20 \mu Hz$ to $70 \mu Hz$, together with the CESAM evolutionary track for models ranging to $1.6 M_{\odot}$ to $4.0 M_{\odot}$.

This relations can be used to have an expected range of the large frequency separation of an observed pulsating PMS star if the position in the HR diagram is known. In the next section this fit will be used as the first step of a methodology to characterize a PMS δ Scuti pulsator on the basis of the pulsation models and the observed frequencies.

4.2 A methodology to reproduce the observed frequencies

On the basis of the linear fit obtained in the previous section, I present a method to compare the observed pulsation frequencies, as well as to obtain information on the stellar structure and physical parameters, such as the mass, the radius, the effective temperature and the age. To summarize my approach, the steps I follow are:

- to combine the grid of models with the known luminosity and effective temperature to determine a range in mass and in the expected large frequency separation;
- to estimate the large frequency separation from the frequency data;
- to reduce the mass range by using the observed large frequency separation;
- to use a few models within the possible range of mass and large separation to reproduce the frequencies in the echelle diagram;
- based on the best representation of the observed frequencies in the echelle diagram to provide the preferred stellar parameters and a tentative mode identification.

The capability of this method has been verified by applying it to “test “stars. In particular I show the application at two test stars, namely “*Star1*” and “*Star2*”. The first one, *Star1* corresponds to a model computed using the STAROX code (Roxburgh, 2005), while the second one, *Star2*, was obtained with the CESAM code (Morel, 1997) after integration of the birthline of Palla & Stahler (1993). The parameters characterising these models are given in Table 4.1.

I notice that two different evolutionary codes have been adopted for producing the two test objects, also changing the initial conditions in one of these, because to I need to ensure that the method does not depend on the adopted evolutionary codes. Then it has been computed the radial and non radial p and g pulsation modes, for the two test stars, by using the POSC code (Monteiro, 1996). The Values of the

Table 4.1: Physical properties (exact values) of the two test stars, and ‘Observed’ values simulations.

	Mass	Radius	Luminosity	$\log(T_{eff})$	Age
	M/M_{\odot}	R/R_{\odot}	$\log(L/L_{\odot})$	K	My
Exact values:					
<i>Star1</i>	2.0	1.862	1.1942	3.9251	0.00
<i>Star2</i>	2.4	3.482	1.5915	3.8887	3.72
‘Observed’ values:					
<i>Star1</i>			1.19 ± 0.82	3.92 ± 0.06	
<i>Star2</i>			1.58 ± 0.07	3.88 ± 0.05	

frequencies, the spherical harmonic degree l and the radial order n are reported in Table 4.2. In both test cases the number of frequencies is high (10 or more) and with a few of those already in the asymptotic regime. Present data on PMS δ Scuti stars are not so rich (only a few frequencies) but forthcoming observations, as for example, from CoRoT, are expected to provide several tens of frequencies per star. In the frequency calculations, again it has been used a different oscillation code, for ensuring that the use of the same code, for the test stars and the reference models used in this work, is not the dominant factor determining the success of the inversion procedure.

These test stars are “theoretically built” by one member of my group, that knew the real stellar parameters and the “real” frequencies reported respectively in Tables 4.1, 4.2. In particular he has simulated real data by shifting the frequencies, the luminosity and the effective temperature relatively to the exact values and quoting an error in some cases not consistent with the original (exact) value. The simulated observations, as reported in Tables 4.1, 4.2, were the only data available to me. I have applied the proposed method to these test data by trying to find the best solution reproducing the observed stellar parameters and frequencies, just as if they were true observed data.

Table 4.2: Frequencies, spherical harmonic degree, and the radial order as computed using the POSC code for the two test stars. In the last column the ‘observed frequencies provided as observables for the two test stars are also given.

	$\nu_{n,l}$ μHz	l	n	‘Observed’ f_i μHz
<i>Star1</i>				
f_1	428.4412	0	5	429 ± 4.5
f_2	493.4204	0	6	493 ± 4.5
f_3	526.5400	1	6	521 ± 4.5
f_4	553.4227	2	6	553 ± 4.5
f_5	591.5814	1	7	594 ± 4.5
f_6	623.5623	0	8	623 ± 4.5
f_7	655.9865	1	8	658 ± 4.5
f_8	683.0216	2	8	682 ± 4.5
f_9	748.6396	2	9	749 ± 4.5
f_{10}	754.4297	0	10	755 ± 4.5
<i>Star2</i>				
f_1	67.1478	1	-2	68 ± 3.5
f_2	83.9724	0	1	84 ± 3.5
f_3	108.1624	0	2	108 ± 3.5
f_4	112.4021	1	1	111 ± 3.5
f_5	134.5490	0	3	134 ± 3.5
f_6	168.5343	1	3	166 ± 3.5
f_7	183.7885	2	4	183 ± 3.5
f_8	188.1748	0	5	188 ± 3.5
f_9	196.8293	1	5	196 ± 3.5
f_{10}	224.3726	1	6	224 ± 3.5
f_{11}	240.7379	0	7	242 ± 3.5
f_{12}	265.4323	0	8	266 ± 3.5
f_{13}	268.3870	2	7	268 ± 3.5
f_{14}	294.3213	2	8	293 ± 3.5
f_{15}	296.9251	0	9	297 ± 3.5

4.2.1 The HR diagram

As mentioned above the first step of the method consists in evaluating the range in mass and large separation of a pulsating PMS δ Scuti stars, by means of its esti-

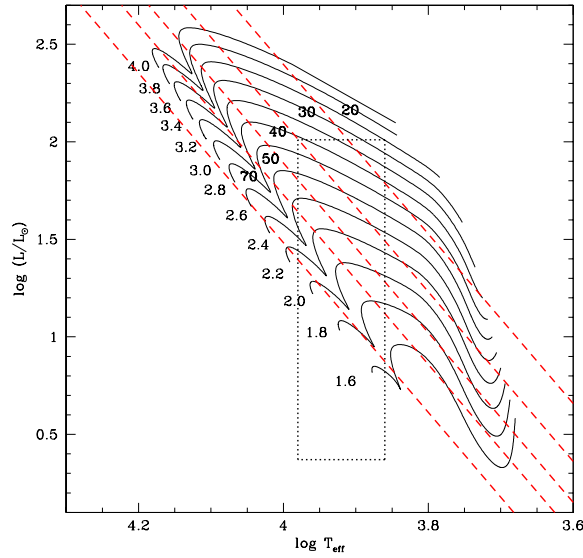


Figure 4.3: Estimated HR diagram position of *Star1* (dotted square) together with the CESAM PMS evolutionary tracks (full lines, for the labelled masses in M_{\odot}) and the linear fit (dashed lines, labelled with $\Delta\nu$ in μHz) of constant large frequency separation obtained in Section 4.1.

mated position in the HR diagram and using the linear fit computed in the previous section. For this purpose I report in the figures 4.3 and 4.4, the predicted HR diagram position for the two test stars *Star1* and *Star2* respectively. In the same plots I also display the set of PMS evolutionary tracks from CESAM for stellar masses ranging from 1.6 to 4.0 solar masses, together with the linear fit for constant large separation (ranging from 20 to 70 μHz).

These plots allow me to define the range in mass consistent with each star and also to determine the possible range of values for the large separation. The obtained mass and large separation ranges are:

$$\textit{Star1}: 1.6 \leq M/M_{\odot} \leq 3.4 \text{ and } 20 \mu Hz \leq \Delta\nu \leq 80 \mu Hz,$$

$$\textit{Star2}: 2.2 \leq M/M_{\odot} \leq 2.8 \text{ and } 20 \mu Hz \leq \Delta\nu \leq 50 \mu Hz.$$

These are quite wide ranges corresponding to the uncertainty on stellar mass when only the classical observables (luminosity and effective temperature) are available. However these ranges could be reduced if it is known another observables, as for example the large separation. This occurrence will be analyzed in the next section.

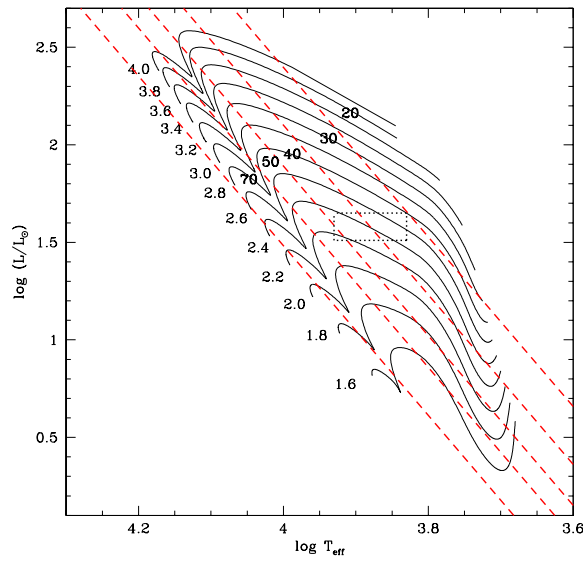


Figure 4.4: The same as Fig. 4.3, but for *Star2*.

4.2.2 The large frequency separation and the echelle diagram

For real stars, the large separation would be ideally extracted directly from the power spectrum of the light curve based on the expected range reported above.

For the test cases there is not a power spectrum, so I have estimated the large separation by studying the regularity of the spacing between the frequencies. In particular, I have plotted the “observed” frequencies in the echelle diagram varying the large separation in the ranges evaluated above, until the best alignment is obtained. The use of the echelle diagram is convenient to illustrate in detail the properties of the frequency spectrum. In this kind of diagram the frequencies are reduced modulo $\Delta\nu$ by expressing them as: $\nu_{nl} = \nu_0 + k\Delta\nu + \tilde{\nu}$, where $\Delta\nu$ is the large separation, ν_0 is a suitably chosen reference frequency, and k is an integer such that $\tilde{\nu}$ is between 0 and $\Delta\nu$. The diagram is produced by plotting $\tilde{\nu}$ on the abscissa and $\nu_0 + k\Delta\nu$ on the ordinate. Graphically, this may be thought of as cutting the frequency axis into pieces of length $\Delta\nu$ and stacking them above each other. If the asymptotic relation (4.1) were precisely satisfied, the result would produce points arranged on a set of vertical lines corresponding to the different values of l .

In Fig. 4.5, 4.6, we report the echelle diagrams assuming $\Delta\nu_1 = 65$ and $\Delta\nu_2 = 27.5$ for star1 and star2 respectively.

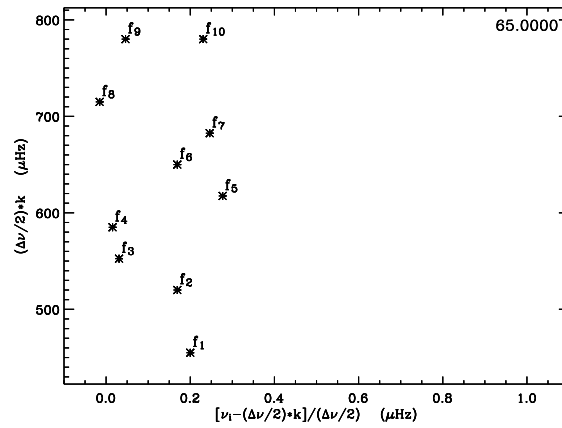


Figure 4.5: Observed echelle diagram for *Star1*.

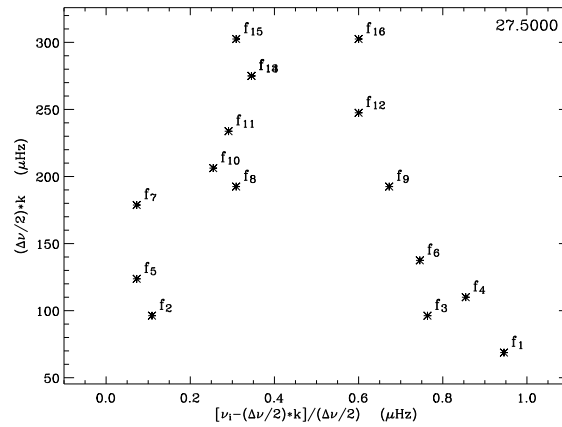


Figure 4.6: The same of fig. 4.5, but for the *Star2*.

From these plots I obtain an indication of the large separations as being about $\Delta\nu_1 \sim 65\mu Hz$ and $\Delta\nu_2 \sim 27\mu Hz$, for *star1* and *Star2*, respectively. This approach does not provide an uncertainty, but in a real case this 'error' could be as high as $\sigma(\Delta\nu) \sim 5\mu Hz$. Using the best values of the large separation, determined above, I can reduce the number of models in the empirical box shown in figures 4.3 and 4.4. In fact I select all the models for which the intersection of the constant lines, around the values of $\Delta\nu_1$, $\Delta\nu_2$, with the evolutionary tracks are inside the assumed uncertainty box. I notice that the knowledge of additional observable ($\Delta\nu$) reduces the number of models to be analyzed.

Only for this subset of models I use the computed frequencies to construct theoretical echelle diagrams and search for the one that best reproduce (i.e. matches as

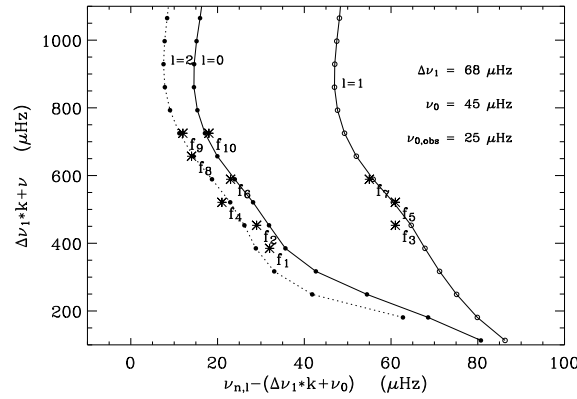


Figure 4.7: Echelle diagram for *Star1*, using the theoretical frequencies computed with the Aarhus code. The parameters used to produce this plot are reported. The observational uncertainties would correspond approximately to the size of the symbols representing the observed frequencies f_i .

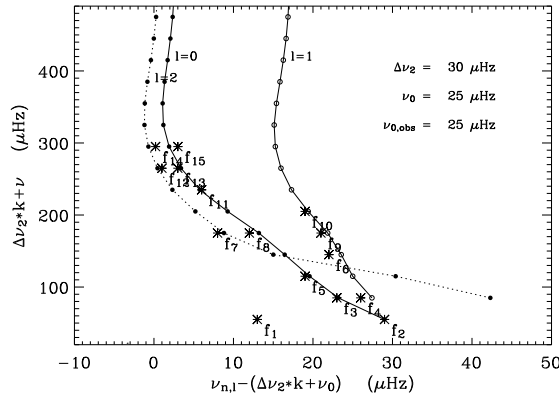


Figure 4.8: The same as Fig. 4.7, but for *Star2*.

many as possible of) the observed frequencies. As a result I obtain ($M = 2.0 M_{\odot}$, $T_{eff} = 8184$ K) for *Star1* and ($M = 2.4 M_{\odot}$, $T_{eff} = 7739$ K) for *Star2*. The corresponding echelle diagrams are shown in Figs 4.7–4.8.

As shown in Fig. 4.7, for *Star1* all the frequencies are reproduced with the best fit model, and all the modes are identified with the correct spherical harmonic degree l and radial order n . The best fit model has also the right mass and an effective temperature that differs from the true one by only 200 K. This is the case with a poorly determined luminosity, but we find that the impact on the mass estimation is weak. Also for *Star2* the method reproduce the right mass and effective temperature and all the 16 frequencies with the right l degree and n order (see Fig. 4.8). The

only exception is f_1 that corresponds to a g mode and this is the reason why the echelle diagram has been unable – correctly – to adjust this particular value, even if the best-fitting model has a g mode that fits f_1 within $0.005 \mu\text{Hz}$. These are both ideal test cases, but they demonstrate that if enough frequencies are known with sufficiently high precision the oscillation spectra can be interpreted using as reference a detailed grid of PMS models and their frequencies as proposed in this work. The key assumption is that the measured values of the frequencies do not deviate strongly from the predicted values and relative spacing.

4.3 Application to observed PMS δ Scuti stars

Once tested the theoretical approach on artificial pulsators, I have tried to evaluate how it can be applied to real observations. The difficulty with ground-based observations of PMS δ Scuti stars is that these do not provide yet a large set of frequencies for each star. But space observations have already been reported where several tens of frequencies with very high precision [?] are measured for a single star. These will be the ideal cases for applying the approach described above.

In the following section I describe the application of the method to two PMS δ Scuti stars, observed by my group during multisites campaigns.

4.3.1 The case of V351 Ori

As a preliminary application I considered the known multiperiodic PMS δ Scuti star V351 Ori (see Marconi et al. 2000, 2001, Balona et al. 2002, Ripepi et al. 2003).

This star has been observed, by my group, with a multisite campaign. In particular six observatories were involved in the observational campaign (see Table 4.3) spanning two years, with a total of around 180 hours of observations over 29 nights.

As a result of this campaign five pulsation frequencies (for detail see Ripepi et al. [58]) have been detected, whose values with the associated uncertainties, are reported in Table 4.4.

Table 4.3: List of telescopes and instrumentations involved in the multisite campaign for the star V351 Ori.

Observatory	Telescope	Instrument
SAAO (S.Africa)	0.5 m	Modular Photometer
Roque de los Muchachos (Spain)	10m JKT	SiTe2 2048x2048 CCD
Beijing Astronomical Observatory(China)	0.85m	Three Channel Photometer
Loiano (Italy)	1.5m	Three Channel Photometer(TTCP)
San Pedro Martir (Mexico)	1.5m	Banish (<i>uvby</i>) Photometer
Kitt Peak National Observatory (USA)	0.9m SARA	512x512 CCD
Teide (Spain)	1.0m OGS	1024x1024 CCD

For the application of the theoretical methodology, the first step is to evaluate the empirical box in the HR diagram. For the effective temperature I have used the value given by van den Ancker et al. 1998 with an uncertainty of $\pm 0.01 dex$, while for the luminosity I use for the lower limit the distance given by Hipparcos, namely of 210 pc, and for the upper limit the distance obtained by assuming that V351 Ori is located in the Orion star forming region. The ranges of luminosity and effective temperature as reported in the literature for V351 Ori are plotted in the HR diagram (dotted box) in Fig. 4.9, together with the PMS evolution tracks. Similarly to the plots presented for the two test stars, I also report in the same diagram the lines at constant large frequency separation. This comparison allows me to obtain a range in mass and large separation consistent with the estimated HR diagram position of the star, namely $1.8 < M/M_{\odot} < 3.0$ and $20 \mu Hz < \Delta\nu_a < 50 \mu Hz$.

In my analysis I mainly focus on reproducing frequencies f_1 , f_2 and f_3 . This assumption is justified by the fact that as noted by Ripepi et al. [58] the first four frequencies are well established, whereas f_5 is slightly less reliable. Moreover f_4 and f_5 are quite close to f_1 and f_3 respectively. As discussed by Breger & Bischof [12] close frequency pairs should be investigated accurately in order to establish whether they are real or not. In particular the quoted authors suggest a method to discriminate which hypothesis (close pair or single mode with amplitude variation)

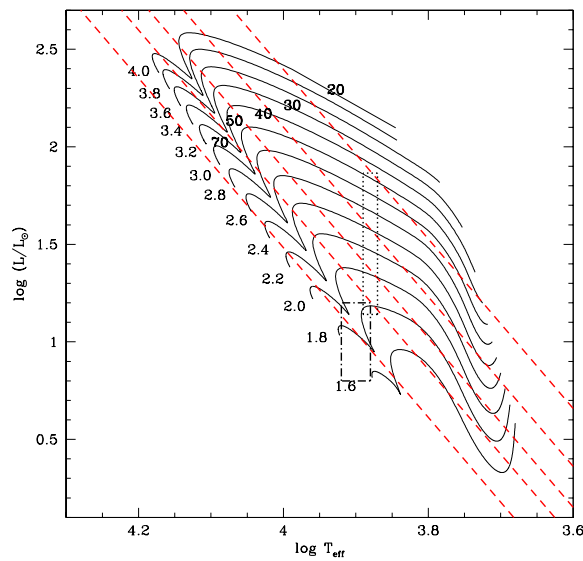


Figure 4.9: The same as Fig. 4.3, but for stars V351 Ori (box with dotted square line), IP Per (box with dot-dashed line).

is correct. Unfortunately, current data on V351 Ori are insufficient to follow this approach.

Table 4.4: Observed frequencies and uncertainties for V351 Ori reported by Ripepi et al. [58].

	Frequency	error
	μHz	μHz
f_1	181.6	0.4
f_2	165.9	0.4
f_3	147.6	0.4
f_4	183.8	0.4
f_5	148.3	0.4

The next step is to identify from the frequency data if a stronger constraint can be posed on the large frequency separation. The large separation of V351 Ori is difficult to estimate directly from the power spectrum, and the number of frequencies is too low for building observed echelle diagram as I have done for the two test stars. So I have used the separations between observed frequencies to evaluate for what

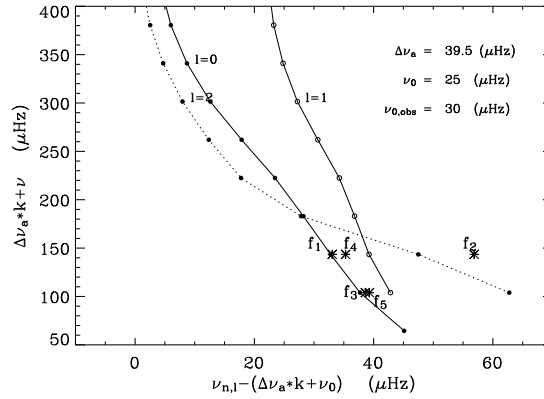


Figure 4.10: The same as figure 4.7, for V351 Ori.

conditions the modes with larger amplitude (expected to be unstable low-order radial modes) are consistent with the range of $\Delta\nu$ found from the HR diagram. By using the reference grid I can extrapolate to the asymptotic regime to find that the frequencies are consistent with a $\Delta\nu_a \sim 40 \mu Hz$.

Consequently, to find the best model that reproduces the observed frequencies I built the theoretical echelle diagram by varying the mass and the large separation within the constraints indicated above. In doing so I assume that the mode with the largest amplitude (f_1) is a radial mode. As a result, I find that the model in the grid consistent with the observed frequencies has a mass $M = 2.0 M_\odot$ and an effective temperature of $T_{eff} = 7539$ K. As shown in the echelle diagram (see Fig. 4.10), the frequencies f_1 and f_3 are associated with radial modes ($l = 0$), namely to the first and second overtone respectively, while f_2 is a nonradial mode (rather close to the $l = 2$ theoretical sequence). As for f_4 and f_5 their position in the echelle diagram is between the $l = 0$ and the $l = 1$ sequences, but as discussed above and in particular for f_5 , the true nature should be investigated carefully on the basis of more extensive data.

There are key assumptions that were made that require further verification. One is the assumption that the highest amplitude mode (f_1) is a radial mode. This is required to properly adjust the echelle diagram to the observed spectrum. This hypothesis, or an equivalent calibration for a radial mode, requires verification from

spectroscopic mode identification.

4.3.2 The case of IP Per

As second application of the method, I have considered the PMS δ Scuti star , IP Per, which has been the target of a recent multisite campaign carried out by my group. ([59]). In this campaign nine telescopes have been involved (see 4.5), with a total of about 190 hours of observations over 38 nights.

Table 4.5: List of telescopes and instrumentations involved in the multisite campaign for the star IP Per.

Observatory	Telescope	Instrument
Loiano (Italy)	1.5m	Three Channel Photometer(TTCP)
Loiano (Italy)	1.5m	BFOSCO
Beijing Astronomical Observatory(China)	0.85m	Three Channel Photometer
San Pedro Martir (Mexico)	1.5m	Banish (<i>uvby</i>) Photometer
SARA(USA)	0.9	CCD
Teide (Spain)	1.0m OGS	1024x1024 CCD
Fairborn(USA)	0.75m T6	SCP
OSN(Spain)	0.9m	<i>uvby</i> Phot.
Serra la Nave	0.9m	SCP
SOAO(Korea)	0.6m	CCD

As a result nine pulsation frequencies (for detail see [59]) have been measured. The corresponding values and the associated uncertainties are listed in Table 4.6.

For the empirical HR diagram position I have used the effective temperature given by Miroschnichenko et al. (2001), that is $T_{eff} \sim 8000 \pm 1000K$ and the luminosity obtained by using the distance given by de Zeeuw et al. 1999 ($D \simeq 300pc, \log L/L_{\odot} \sim 1$). The estimated position (box with dot-dashed lines) of IP Per in the HR diagram is shown in Fig. 4.9, together with the reference grid of PMS evolutionary tracks. From this plot I can restrict the mass and large separation expected for this star to

the ranges $1.6 < M/M_{\odot} < 2$ and $50 \mu Hz < \Delta\nu_b < 75 \mu Hz$.

Table 4.6: Observed frequencies and uncertainties for IP Per reported by [59].

	Frequency error	
	μHz	μHz
f_1	264.9	1.3
f_2	400.5	1.3
f_3	352.4	1.3
f_4	558.2	1.3
f_5	333.2	1.3
f_6	277.6	1.3
f_7	107.6	1.3
f_8	487.4	1.3
f_9	602.3	1.3

Due to the higher number of modes, and considering that five of these have a large amplitude, the separation between observed frequencies indicates that the data are consistent, within the expected range, with $\Delta\nu_b \sim 50 \mu Hz$ when extrapolated to the asymptotic regime. Following these constraints I have then used the echelle diagram to find the best stellar mass and age that reproduce as many as possible of the observed frequencies. As a result we find a best fit model with $M = 1.8 M_{\odot}$, and $T_{eff} = 7773$ K. The corresponding echelle diagram is shown in Fig. 4.11.

According to this plot, frequencies from f_1 to f_4 seem to align along the sequence for $l = 0$ modes, whereas f_5 , f_6 and f_8 are better in agreement with $l = 1$ theoretical predictions, and f_9 could be an $l = 2$ mode. The discrepancy between the theoretical and observed frequencies is probably due to a residual uncertainty on stellar mass, intrinsic to the adopted model grid. A slightly lower mass would probably allow us to better reproduce the observed frequencies in the echelle diagram. In any case the frequency f_7 is not consistent with a p mode as it lies well below the expected frequencies for the range of stellar masses of IP Per. This frequency could correspond to a g mode, but this hypothesis had been confirmed.

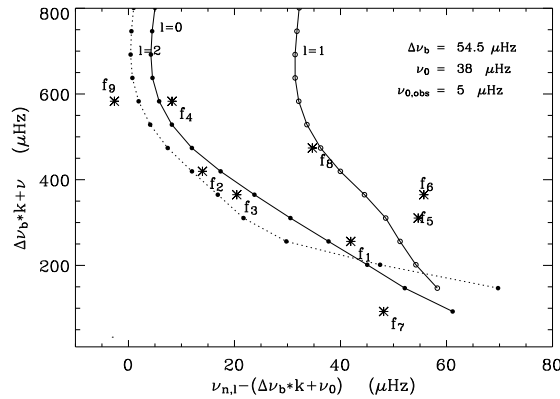


Figure 4.11: The same as figure 4.7, for IP Per.

4.4 Effects of rotation

The rotation of PMS δ Scuti stars is an important factor to be considered in the mode identification.

On the basis of the asymptotic relation rotation is expected to produce a splitting of the "unperturbed" modes. This frequency displacement is given by:

$$\Delta f = m f_{rot} = m \frac{(v_{rot} \sin i)}{(2\pi R \sin i)} \quad (4.4)$$

where $-l < m < l$ is the harmonic number, v_{rot} is the rotational velocity, i the inclination angle and R the stellar radius. I have used this relation to evaluate the rotational splitting of the modes, of V351 Ori, for which estimates of a relatively high rotational velocity are given in the literature. In particular I have used the value estimated by Balona et al. (2002) ($v \sin i \simeq 100$ km/sec), that gives a displacement of the order of $8m / \sin i \mu Hz$. Such a relatively large splitting removes the possibility that the separation between f_4 and f_1 and between f_3 and f_5 is due to rotation, once the hypothesis of radial modes for f_1 and f_3 is abandoned. However, f_2 is shifted by about $10 \mu Hz$ from the predicted frequency, which may correspond to a $m \neq 0$ mode, pending spectroscopic confirmation. It should also be noted that for such a relatively rapid rotation higher-order effects must be taken into account [e.g., 22, 29, 67]. These would lead to non-uniform splitting and shifts of modes with $m = 0$, including the radial modes. It is likely that such rotational frequency perturbations will be a substantial complication in the analysis of oscillations of

PMS stars, which typically are rapid rotators.

Connection to the ESTA CoRoT activity

In this chapter I present the contribution of my PhD thesis to the *Evolution and Seismic Tools* Activity (ESTA) in the context of the CoRoT mission.

5.1 CoRoT ESTA

The CoRoT ESTA is a seismology working devoted to the preparation and exploration of the scientific results of CoRoT concerning stellar oscillations. To this purpose the ESTA aims at:

- providing a grid of reference stellar models and their frequencies of oscillations, by means of different numerical codes;
- testing, comparing and optimizing numerical tools used to calculate stellar models, oscillations frequencies and seismic inversions.

In particular the ESTA can rely on seven different evolutionary codes and eight different pulsational codes (see 5.1).

Table 5.1: Evolutionary and pulsational codes used in the context of ESTA collaborations. comparison.

name	references
ASTECC	Cristensen-Dalgaard(1982, 2005)
CESAM	Morel(1997) and Pichon & Morel (2005)
CL 'ES	Scuflaire (2005)
FRANEC	Cariulo et al. (2004) and Degl' Innocenti & Marconi (2005)
GENEC	Meynet & Maeder (2000)
STAROX	Roxburg (2005a,b)
TGEC	Richard et al. (1996) and Castro (2005).
ADIPLS	(http://astro.phys.au.dk/~jcd/adipack.n/)
FILOU	Sua'rez (2002)
GRACO	Moya et al. (2004)
LOSC	Boury et al. (1975); Scuflaire (2005)
NOC	Unno et al. (1989)
OSCROX	Roxburg(2005b)
POSC	(http://www.astro.up.pt/~mjm/)
ROMOSC	Suran et al. (1991)

My group enters the CoRoT ESTA with the FRANEC code, and the ADIPLS code, adapted in this thesis for the first time to PMS δ Scuti stars.

The first step of ESTA consists in comparing stellar models and evolution sequences produced by the seven participating evolutionary codes (see Monteiro et al. 2006). While the second consist of testing, comparing and optimising the seismic codes by comparing the frequencies produced by different oscillation codes. In the next sections I discuss the results already obtained for these two steps.

5.2 Comparisons among evolutionary codes

For comparing the stellar models produced by the different groups, the same physical assumption has been adopted by the different codes . In particular

- Rotation and magnetic field are neglected;
- The adopted equation of state is the OPAL2001 (Rogers & Nayfonov, 2002), that is provided in a tabular form;
- The opacities used are the OPAL95 opacities tables (Iglesias & Rogers, 1996) complemented at low temperatures by Alexander & Ferguson (1994) tables;
- For the reaction rates the basic pp and CNO reaction networks up to the $^{17}\text{O}(p, \alpha)^{14}\text{N}$ reaction are used. The nuclear reaction rates are computed using the analytical formulae provided by the NACRE compilation (Angulo et al., 1999).
- For the convection and overshooting the classical mixing length treatment of Böhm-Vitense (1958) under the formulation of Henyey et al. (1965) is used;
- For the atmosphere the Eddington’s grey $T(\tau)$ law ($T = T_{eff}[\frac{3}{4}(\tau + \frac{2}{3})^{\frac{1}{4}}$) where τ is the optical depth, is used. The level where the integration of the hydrostatic equation starts depends on the codes as well as the level where the atmosphere is matched to the envelope. The radius of the star is taken the bolometric radius, i.e., the radius where the local temperature equals the effective temperature;
- For the initial abundances of the elements, the models are calculated with the classical Grevesse & Noels (1993) solar mixture of heavy elements.

Models have been selected as reported in table 5.2. The comparison of the evolutionary tracks for these models, computed with the various codes, is reported in Figs. 5.1 - 5.7. Similar comparisons for relevant physics quantities can be found in Moneiro et al. 2006, and are available upon request.

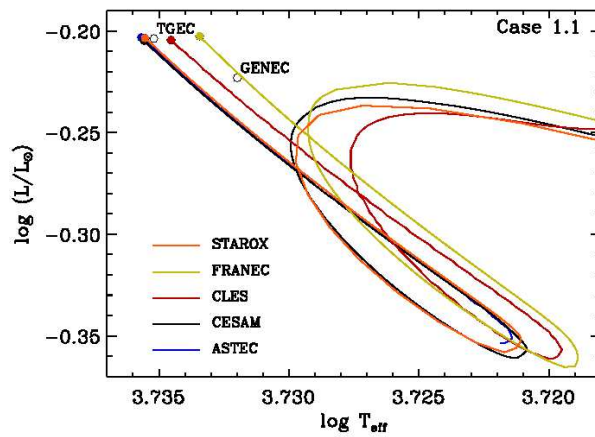


Figure 5.1: Comparison of the evolutionary track computed with the different code disponible in the context of CoRoT ESTA for the models 1.1.

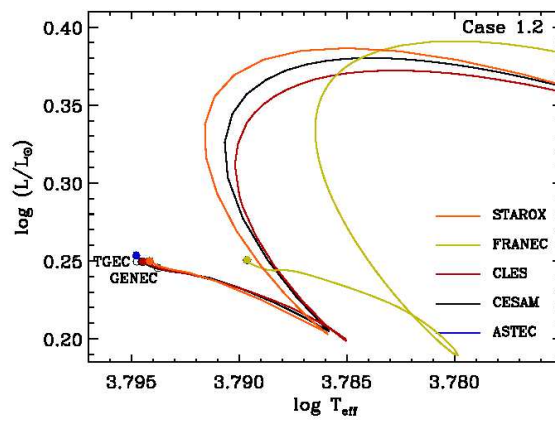


Figure 5.2: The same as Fig. 5.1 for the models 1.2.

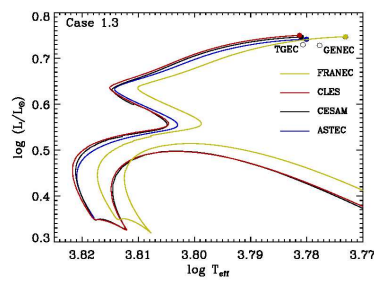


Figure 5.3: The same as Fig. 5.1 for the models 1.3.

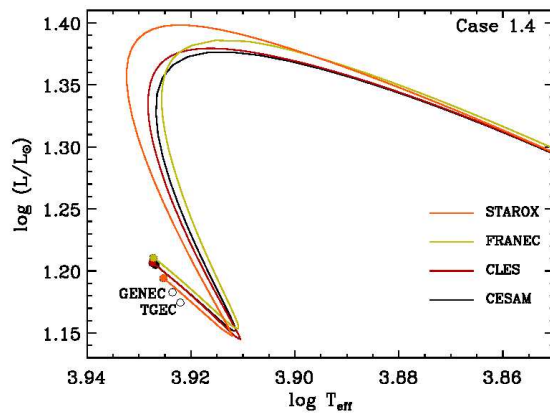


Figure 5.4: The same as Fig. 5.1 for the models 1.4.

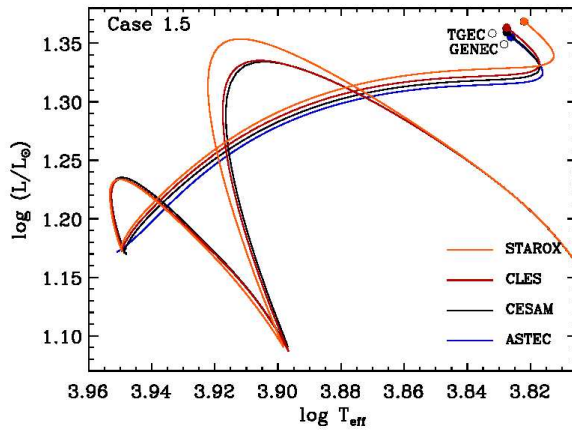


Figure 5.5: The same as Fig. 5.1 for the models 1.5.

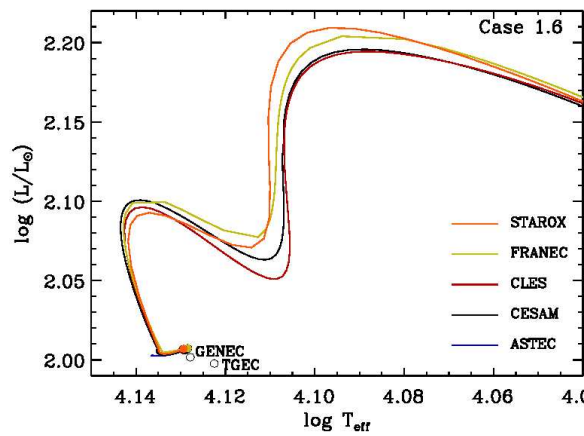


Figure 5.6: The same as Fig. 5.1 for the models 1.6.

Table 5.2: Models used for ESTA comparisons. In the columns I report: the name of the models, than the masses (M) in units of solar mass (M_{\odot}), the helium abundance, the metal abundance, the central hydrogenum, the central effective temperature in K, the mass of the helium core in units of solar mass (M_{\odot}), the overshooting parameters, and the evolutionary phase. while the temperature is in K.

Case	M	Y_0	Z_0	X_c	T_c	Mass H_e core	overshoot	Type
1.1	0.9	0.28	0.02	0.35	-	-	-	MS
1.2	1.2	0.28	0.02	0.69	-	-	-	ZAMAS
1.3	1.2	0.26	0.01	-	-	0.1	-	Post-MS
1.4	2.0	0.28	0.02	-	1.9×10^7	-	-	Pre-MS
1.5	2.0	0.26	0.02	0.01	-	-	0.15 Hp	TAMS
1.6	3.0	0.28	0.01	0.69	-	-	-	ZAMS
1.7	5.0	0.28	0.02	0.35	-	-	-	MS

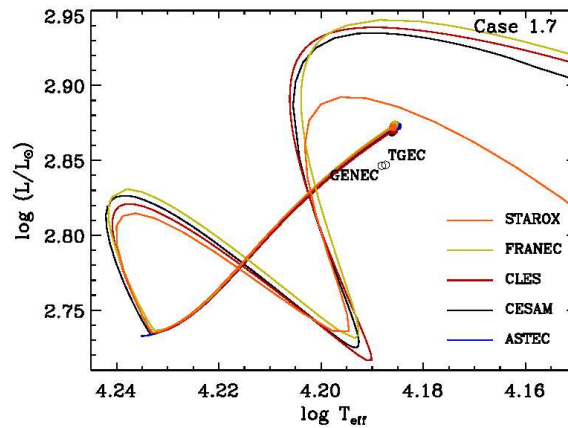


Figure 5.7: The same as Fig. 5.1 for the models 1.7.

5.3 Pulsational frequency comparison

For the comparison of seismic properties I have first compared the frequencies obtained with the ADIPLS and POSC codes for the models 1.1 and 1.4 computed with the CESAM code. For this purpose I have computed the p mode frequencies for $l = 0, 1, 2$ for $n = 2, 26$, for both models and compared then with the one's obtained with the POSC code.

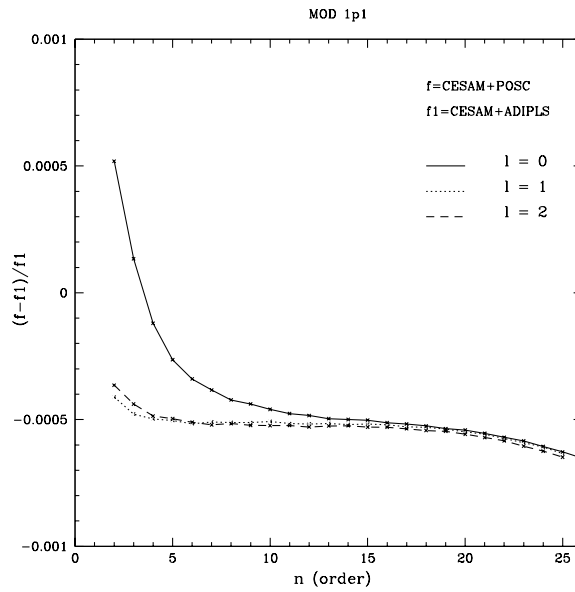


Figure 5.8: Relative difference between the frequencies computed with the POSC code and the ADIPLS ones for the models 1.1. The comparison is performed for p modes ($l = 0, 1, 2$) and for the radial order ranging from 2 to 26.

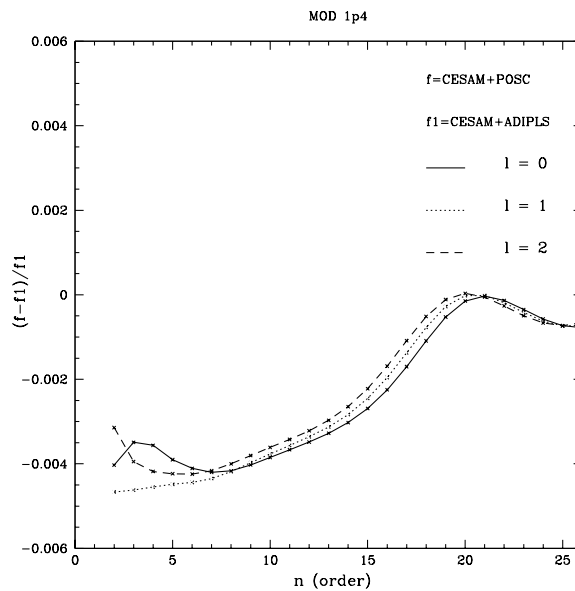


Figure 5.9: The same as 5.8, but for the model 1.4.

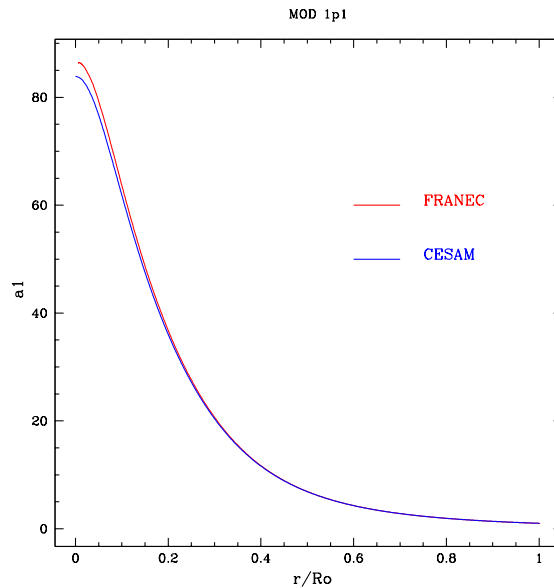


Figure 5.10: Comparison of the a_1 quantity for the model 1.1 of ESTA CoRoT. FRANEC results are in red, the CESAM ones in blue.

As shown in Figures 5.8 - 5.9 the p mode frequencies computed with the two different codes are in agreement to less than 0.05%. This comparison allows us to verify that the two pulsational codes are in very good agreement. As a second step I have applied the ADIPLS pulsation code to the models 1.1 and 1.4 computed with the FRANEC evolutionary code.

Before comparing the resulting frequencies with the corresponding ones obtained from the CESAM models I have compared the a_i 's quantities, (see equations 3.6). Figure 5.10 shows the comparison of the a_1 quantity based on FRANEC and the same quantity based on CESAM for the model 1.1. We notice that the differences are very small except for the central region of the star where they can reach a few percent. We notice that a_1 is related to the density (see 3.6) so that the quoted difference in central zone corresponds to a residual difference in the density profile between the two evolutionary models.

Figure 5.11 shows the comparison for the a_2 quantity. It is linked to the mass, the pressure, the density and the radius of the stars (see 3.6), that can be obtained easily as an output of both the code. The differences between the CESAM and FRANEC

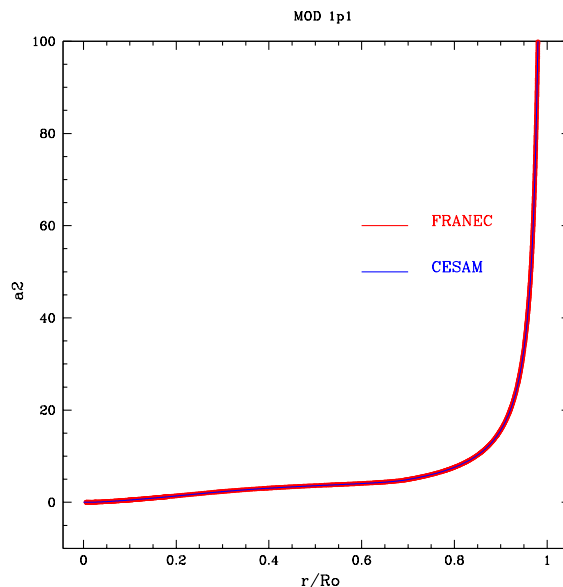


Figure 5.11: The same as 5.10, but for the a_2 quantity.

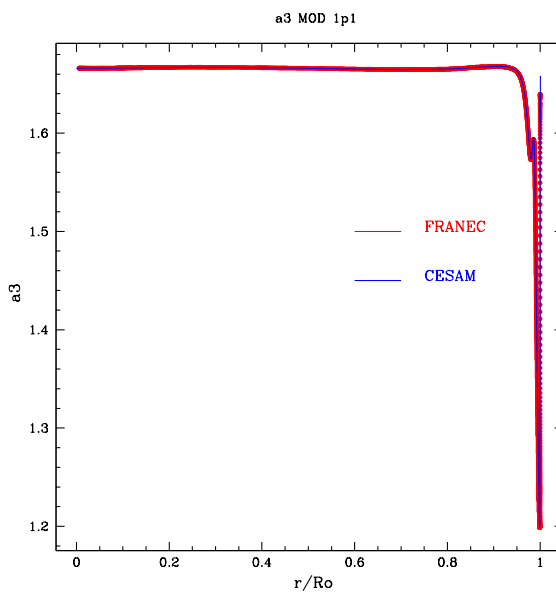


Figure 5.12: The same as 5.10, but for the a_3 quantity.

results also in this case are less than 2%.

The a_3 quantity is Γ_1 , and the differences between the two code predictions remain less than 4% (see figure 5.12).

The computation of the a_4 quantity is more complex. In fact a_4 is defined as $a_4 = \frac{-1}{\Gamma_1} \frac{d \ln P}{d \ln r} - \frac{d \ln \rho}{d \ln r}$. The first term can be evaluated by means of the hydrostatic equilibrium condition. The second term $\frac{d \ln \rho}{d \ln r}$ is evaluated in the CESAM code, by

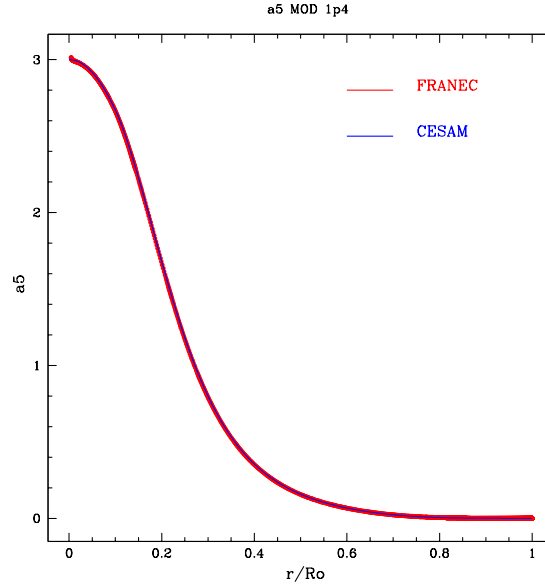


Figure 5.13: The same as 5.10, but for the a_4 quantity.

approximating the derivative of the density as follows :

$$\frac{d \ln \rho}{d \ln r} = \alpha \frac{d \ln P}{d \ln r} - \delta \frac{d \ln T}{d \ln r} + \phi \frac{d \ln \mu}{d \ln r} \quad (5.1)$$

where $\phi = \frac{\partial \ln \rho}{\partial \ln \mu} = 1$ and $\frac{1}{\Gamma_1} = \alpha - \delta \nabla_a d$. On this basis the a_4 becomes:

$$a_4 = \delta (\nabla - \nabla_a d) \frac{\partial \ln P}{\partial \ln R} - \phi \frac{\partial \ln \mu}{\partial \ln R} \quad (5.2)$$

For the computation of this relation the derivatives of all the chemical species with respect to the radius are needed. This requirement is not verified by the FRANEC code, so I computed the a_4 quantity as follows:

$$a_4 = -\frac{GM\rho}{\Gamma_1 p r} - r^3 4\pi \frac{dm}{d\rho} \quad (5.3)$$

where the mass has been interpolated as a function of ρ with a spline.

The comparison between the a_4 quantities obtained with the CESAM and FRANEC codes is shown in figure 5.13 for the model 1.1. The differences between FRANEC and CESAM are more evident in the atmosphere as shown by the zoom plotted in Fig. 5.13.

Finally the comparison of the a_5 quantity (given by $\frac{4\pi\rho r^3}{m}$) is shown in figure 5.14, showing an agreement within 1%.

Similar results have been obtained for the model 1.4 and are available upon request. .

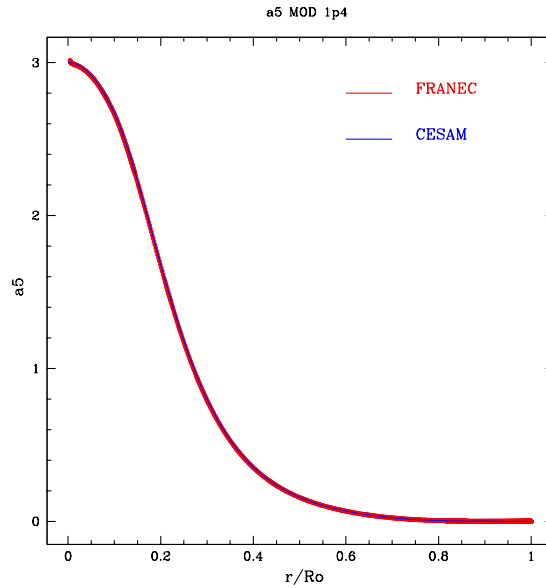


Figure 5.14: The same as 5.10, but for the a_5 quantity.

As second step I have computed the frequencies using the ADIPLS code for the models 1.1 and 1.4 either computed with the CESAM code or with the FRANEC code . Figures 5.15 5.16 show the relative differences between the frequencies obtained for both the models with the harmonic degree ranging from $l = 0$ to $l = 2$ and the radial order from $n = 2$ to 26.

The differences appear to be more significant at low radial order suggesting either some difference in the numerical treatment of some physical ingredients or a non negligible role of the discrepancies found for the a_i .

5.4 FRANEC PMS evolutionary models

One of the objectives of the CoRoT ESTA is to provide reference grid of evolutionary models. Moreover we are interested in optimizing FRANEC to asteroseismological purposes and also to use it in the future in our interpretation techniques applied to PMD δ Scuti stars. For these reasons we have computed a fine grid of PMS evolutionary tracks, for the stellar masses ranging from 1.5 to 4 M_{\odot} and for solar chemical composition (see Fig. 5.17).

Several structure models will be selected along each evolutionary track and used to

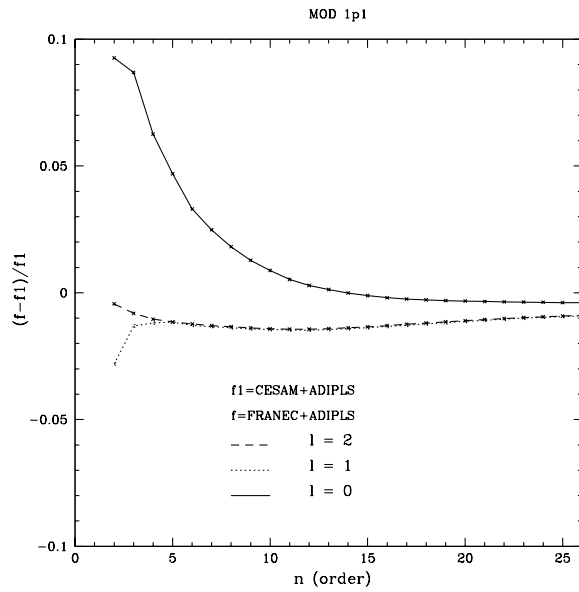


Figure 5.15: Relative difference between the frequencies computed with the ADIPLS code for the model 1.1 obtained with FRANEC and CESAM code. The comparison is performed for p mode ($l = 0, 1, 2$) and for the radial order ranging between 2 and 26.

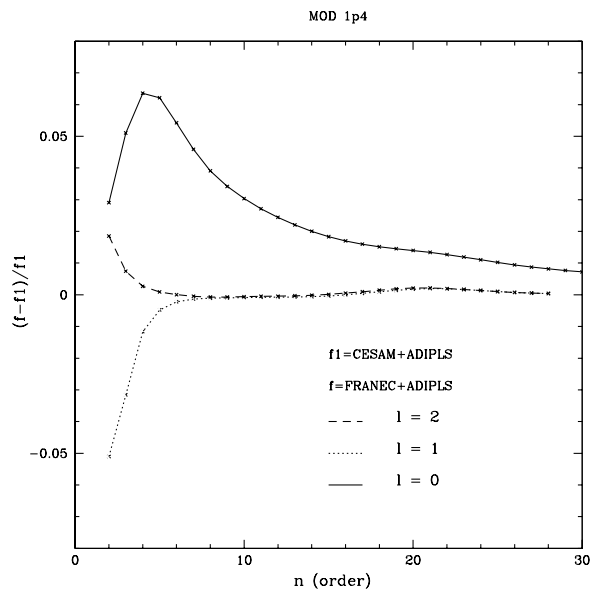


Figure 5.16: The same as 5.15, but for the model 1.4.

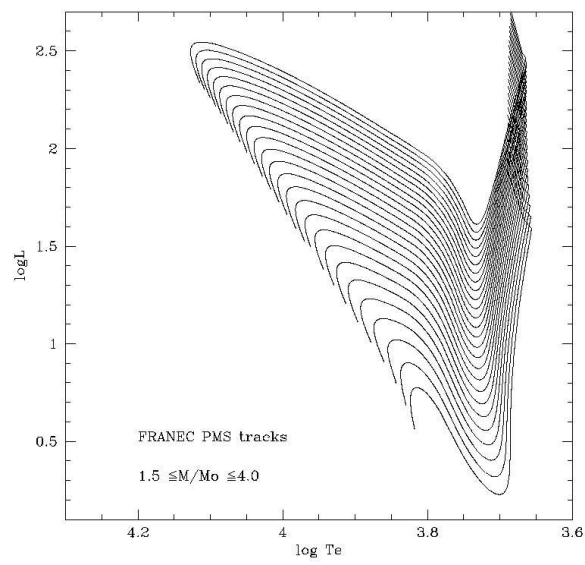


Figure 5.17: PMS Evolutionary tracks computed with the FRANEC code.

compute a fine grid of pulsational frequencies.

Conclusion and future prospect

In this thesis I have analysed the pulsation properties of PMS δ Scuti stars from the theoretical point of view. In the context of a growing observational interest for this kind of pulsators and increasing evidences of the simultaneous presence of radial and non radial modes in these objects, I have started a theoretical project devoted to the interpretation of the observed behaviours. I have adapted an existing non radial linear adiabatic code, originally developed by Christensen Dalsgaard for the sun, to PMS intermediate mass stars and I have applied it to PMS evolutionary models existing in the literature. The behaviour of the theoretical frequencies as a function of the mass and stellar radius has been investigated. As a first application I have compared the theoretical periodicities with the observed ones for the PMS δ Scuti star VV Ser, observed by my research group. In order to compare the extracted periodicities with model predictions, we have considered a large empirical range both in luminosity and effective temperature, reflecting the existing uncertainties on the stellar properties. Within this space of physical parameters, we have computed a fine grid of inner structure models along the CESAM evolutionary tracks. The corresponding pulsation frequencies for $l=0,1,2$ modes have been compared with the observed ones by requiring an agreement within $2.5 \mu\text{Hz}$. As a

result, we have found a number of best fit models corresponding to PMS stars with mass in the range $3.6\text{--}4.0 M_{\odot}$ and luminosity $\log L/L_{\odot} \approx 2.1\text{--}2.3$, that reproduce all the observed periodicities with radial and/or nonradial p and g modes. Such an independent confirmation of the fundamental stellar parameters range previously estimated for VV Ser is an important byproduct of the main objective of asteroseismology, i.e. of sensing the internal structure of the star. We also notice that if the effective temperature is significantly lower (~ 7000 K) than the values based on the empirical spectral types ($\simeq 9000$ K), we are able to reproduce all the observed periodicities with p modes for a stellar mass of $4 M_{\odot}$ and a luminosity of $125 L_{\odot}$. To investigate in more detail the pulsational properties of the PMS δ Scuti stars, a procedure has been developed, based on an extended grid of models and oscillation frequencies to compare the observed periodicities with the theoretical ones in order to constrain the physical properties, such as the mass, radius and the age, of this class of objects. The procedure uses a grid of PMS evolutionary models to identify in the HR diagram the range of stellar masses. From the frequencies we estimate the large frequency separation which is then used to reduce the uncertainty on stellar mass. Finally, from the detailed analysis of the echelle diagram for the few possible combinations of mass/age, a fit of as many observed frequencies as possible is obtained. The underlying principle of this approach is to extract sequentially the information from the frequencies that are more robust and directly connected to the global parameters, reducing in this way as much as possible the effect of the unknown physics in this type of stars. I also notice that the proposed method is quite general, as it can be applied by using models computed with any evolutionary code. In order to evaluate the validity of the proposed approach I have considered two test cases for which estimates of the luminosity and the effective temperature have been simulated together with a set of frequencies given with realistic uncertainties. In both cases the result was positive, and the parameters were recovered with considerable precision even when the luminosity of the stars was poorly known. The consistency between the true and the inferred stellar parameters for both star 1 (computed with STAROX) and star 2 (computed with CESAM), seems to indicate that the method does not depend on the adopted evolutionary

code. A comparison with other evolutionary codes (e.g. FRANEC, ATON, Siess et al. 2000) will be performed when a large number of accurate frequencies, as expected from CoRoT observations, will be available for PMS δ Scuti stars. The method proposed is mainly aimed at studying stars whose pulsation data include several tens of frequencies, as it is expected to be obtained by CoRoT in the near future. However, I have also considered the possibility of applying it to stars whose frequency spectrum includes a smaller number of measured frequencies. To do so I have reported the preliminary applications to two stars that have been targets of multisite campaigns: V351 Ori and IP Per. The uniqueness of the solution is strongly dependent on the number of frequencies being used when these are less than about ten.

However, the results illustrate the capability of this approach to constrain the stellar parameters, and in particular the stellar mass, even when a small number of frequencies is available. For a higher number of frequencies the stellar mass and age could be constrained and the frequencies used to test the physics of the models. The application to a much larger number of frequencies for PMS pulsators (in particular as expected from space observations) and the adoption of finer model grids could considerably improve our knowledge of the stellar properties and structure in this very important phase of stellar evolution. A comparison with other evolutionary codes (e.g. FRANEC, ATON, Siess et al. 2000), as planned in the context of the CoRoT/ESTA collaboration, will also be investigated.

I have also presented the work done in the context of the CoRoT/ESTA. In particular I have compared the results obtained by the FRANEC code with the ones based on different evolutionary codes for modelling the same selected stellar models. It has been verified that some differences persist in spite of the adoption of similar physical inputs, but also that a good agreement is found for the overall behaviour. Once tested the similarities between the different evolutionary code, I have applied two pulsation codes, namely ADIPLS and POSC the same CESAM model. The resulting frequencies are in agreement to less than 0.05%. Then, to verify that the combination FRANEC plus ADIPLS is good for computing asteroseismological models I have applied the ADIPLS code to FRANEC and CESAM models for the

same stellar cases. The results show that some significant differences between the CESAM plus ADIPLS and FRANEC plus ADIPLS model frequencies remain, in particular at low radial orders. We plan to investigate in detail the precise causes of this discrepancy and to complete the optimization of the FRANEC code for asteroseismological purposes. Moreover, we plan to compute radial and non radial theoretical frequencies for a fine grid of stellar structures along the PMS evolutionary tracks computed with the FRANEC code in the final period of my thesis, in order to provide an alternative theoretical framework..

References

[5] Alexander, D. R., Fergusson, J. W. 1994, ApJ, 437, 879

[2] Acke & van den Ancker (2004)

[3] Alecian, E., Catala, C., van't Veer-Menneret et al. 2005, A & A, 442, 993A

[4] Alecian, E., Goupil, M.-J., Lebreton, Y. 2006, IAUS, 240E, 176A

[5] Alexander, D. R., Fergusson, J. W. 1994, ApJ, 437, 879

[6] Angulo C., Arnould M., Rayet M., et al., 1999, Nuclear Physics A, 656,3

[7] Baglin, A., Barban, C., Goupil, M.-J., Michel, E., Auvergne, M. 2000, ASP Conference Series, 210,359

[8] Balona, L. A., Koen, C., van Wyk, F. 2002, MNRAS, 333, 923

[9] Beech, M. & Mitalas, R. 1995, ApJS, 95, 517

[10] Bernasconi, P.A. & Maeder, A. 1996, A & A, 307, 829

[11] Breger, M. 1972, ApJ, 171, 539

[12] Breger, M., Bischof, K. M. 2002, A & A, 385, 537

[Böhm et al. 2004] Böhm, T., Catala, C., Balona, L., Carter, B. 2004, A&A, 427, 907

[13] Boury A., Gabriel M., Noels A. et al. 1975, A & A, 41, 279

[Cariulo et al. 2004] Cariulo P., Degl'Innocenti S., Castellani V. 2004 A& A, 421,1121

[Castro] Castro M. 2005 in CoRoT/ESTA Meeting 4, Aarhus Denmark

- [14] Chavarría-K., C., de Lara, E., Finkenzeller, U., Mendoza, E. E., Ocegueda, J 1988, A & A, 197, 151
- [15] Christensen-Dalsgaard J., 1982, MNRAS, 199,735
- [16] Christensen-Dalsgaard J., 2005, in 2 papers presented at CoRoT/ESTA Meeting 4, Aarhus, Denmark
- [17] Cohen, M. & Kuhl, L. V. 1979, ApJS, 41, 743
- [18] Cowling, T.G. 1941, MNRAS, 101, 367
- [19] de Lara, E., Chavarría-K, C., Lopez-Molina, G. 1991, A & A, 243, 139
- [20] Degl'Innocenti S., Marconi M., 2005 CoRoT/ESTA Meeting 3, Nice, France
- [21] Donati, J.-F., Semel, M., Carter, B. D., Rees, D. E., & Cameron, A. C. 1997, MNRAS, 291, 658
- [22] Dziembowski, W. A. & Goode, P. R. 1992, ApJ, 394, 670
- [23] Eddington, A.S. 1926 *The internal Constitution of the Stars* (Cambridge Univ. Press, Cambridge)
- [24] Ferná'ndez, M., Ortiz, E., Eiroa, c., Miranda, L., F. 1995, A&AS, 114, 439
- [25] Finkenzeller, U. & Mundt, R. 1984 A & AS, 55, 109
- [26] Gabriel, M. & Noels, A., 1976. Acta Astron., 53, 149
- [27] Gray, R. O., Corbally, C. J. 1998, AJ, 116, 2530
- [28] Gough, D.O. 1986 S&T, 72, 479G
- [29] Gough, D. O. & Thompson, M. J. 1990, MNRAS, 242, 25
- [30] Grevesse N., Noels A. 1993, in Origin and Evolution of the Elements
- [31] Grigahcène, A. Duprey, M.-A., Garrido, R., Gabriel, M., Scuflaire, R. 2006, CoAst, 147, 69
- [32] Hayashi, C. 1961, PASJ, 13,450

- [33] Henyey, L.G., LeLevier, R. & Levee, R.D. 1955, PASP, 67,154
- [34] Henyey L., Vardya M.S., Bodenheimer P. 1965, ApJ, 142, 841
- [35] Herbig G. H. 1960, ApJs, 4, 337
- [36] Herna'andez,J., Calvet, N., Brice ò, C., Hartmann, L., Berlind,P. 2004, ApJ, 127, 1682
- [37] Hillenbrand, L.A., Strom, S.E., Vrba, F.J., Keene, J.1992, ApJ, 397, 613
- [38] Iben, I. 1965, ApJ, 141, 993
- [39] Iglesias, C. A. & Rogers, F. J. 1996, ApJ, 464, 943
- [40] Koen, C., Balona, L.A., Khadaroo, K., et al. 2003, MNRAS, 344,5060
- [41] Kurtz, D. W., & Marang, F. 1995, MNRAS, 276, 191
- [42] Marconi, M., & Palla, F. 1998, ApJ, 507, L141
- [43] Marconi, M., Ripepi, V., Alcaá, J.M., Covino, E., Palla, F., Terranegra, L. 2000, A &A, 335, L35
- [44] Marconi, M., Ripepi, V., Bernabei, S., et al. 2001, A & A , 372, 21
- [45] Marques, J.P. 2006, PhD Thesis, Faculdade de ciências da Universidade do Porto
- [46] Meynet G., Maeder A. 2000, A & A, 361, 10
- [47] Monteiro, M.J.P.F.G. 1996, PhD Thesis, Queen Mary College, University of London, UK
- [48] Monteiro, M.J.P.F.G. et al. 2006 Report ON the CoRoT Evolution and seismic tools activity
- [49] Mora, A., Meri'n, B., Solano, E. et al. 2001, A&A, 378, 116
- [50] Morel, P. 1997, A & As, 124, 597
- [51] Moya A., Garrido R., Dupret M.A. 2004, A & A, 414, 1081

- [52] Norberg, P., Maeder, A. 2000, *A & A*, 359 1025N
- [53] Palla, F. & Stahler, S.W. 1991, *ApJ*, 375,288
- [54] Palla, F. & Stahler, S.W. 1993, *ApJ*, 375, 288
- [55] Pichon B., Morel P., 2005, in CoRoT/ESTA Meeting 3, Nice, France
- [56] Racine 1968, *AJ*, 73, 233
- [57] Richard O., Vauclair S., Charbonnel C. et al. 1996, *A A*, 312,1000
- [58] Ripepi, V., Marconi, M., Bernabei, et al. 2003, *A & A*, 408, 1047
- [59] Ripepi, V., Bernabei, S., Marconi, M. et al. 2006, *A & A*, 449, 335
- [60] Rogers, F. J., Swenson, F. J., Iglesias, C. A. 1996, *ApJ*, 456, 902
- [61] Rostopchina, A. N., Grinin, V.P., Shakhovskoi, D.N. 2001, *Astronomy Reports*, 45,60
- [62] Roxburgh, I.W. 2005a, CoRoT/ESTA Meeting 4 (<http://www.astro.up.pt/corot/welcome/m>
- [63] Roxburgh, I.W. 2005a, CoRoT/ESTA Meeting 5, CW9 ESA/ESTEC
- [64] Schmidt-Kaler 1965, in Landolt-Börnstein, Numerical data and functional relationship in science and technology, group VI, vol.I, pp. 284, Springer Verlag, Berlin
- [65] Siess, L., Forestini, M. & Bertout, C. 1997, *A & A*, 308, 472
- [66] Stahler, S. W. 1988, *ApJ*, 332, 804
- [67] Soufi, F., Goupil, M. J. & Dziembowski, W. A. 1998, *A & A*, 334, 911
- [68] Sculfaire R., 2005, in 2 presentations at CoRoT/ESTA Meeting 4, Aarhus, Denmark
- [69] Strom, S.E, Grasdalen, G.L., Strom, K.M. 1974, *ApJ*, 191, 111
- [70] Sua' rez J.C. 2002 PhD Thesis, Observatoire de Paris, Paris 7 University
- [71] Suran M. 1991, *Rom. Astron. J.*, 1, 39

- [72] Suran, M., Goupil, M., Baglin, A. et al. 2001, *A & A*, 372 233
- [73] Tassoul, M. 1980, *ApJs*, 43, 469
- [74] Testi, L., Palla, F., Natta, A 1998 *A & AS*, 133,81
- [75] Unno W., Osaki Y., Ando H. et al 1989, *Nonradial oscillations of stars* (Tokyo: University of Tokyo Press, 2nd ed.)
- [76] van de Ancker, M.E., de Winter, D., Tkin A Djie, H.R.E. 1998, *A & A*, 339,145
- [77] Vieira, S. L.A., Corradi, W.J.B., Alencar, S.H.P. et al. 2003, *AJ*, 126,2971
- [78] Zhevakin, S. A. 1953, *Russian Astron. J.*, 30, 161
- [79] Zwintz K., Marconi M., Reegen, P., Weiss W.W. 2005, *A &A*, 433, 267K